

Circularly polarised lanthanide luminescence for advanced security inks

Lewis E. MacKenzie & Robert Pal[†]

Department of Chemistry, Durham University, Durham, United Kingdom

[†]Email: Robert.Pal@Durham.ac.uk

Abstract | Authenticating products and documents with security inks is vital to global commerce, security and health. Lanthanide complexes are widely used in luminescent security inks due to their unique and robust photophysical properties. Lanthanide complexes can also be engineered to undergo circularly polarised luminescence (CPL), which encodes chiral molecular fingerprints in luminescence spectra that cannot be decoded by conventional optical measurements. However, chiral CPL signals have not yet been exploited as an extra security layer in advanced security inks. This Review introduces CPL and related concepts that are necessary to appreciate the challenges and potential of lanthanide-based CPL-active security inks. We describe recent advances in CPL analysis and read-out technologies that have expedited CPL-active security ink applications. Further, we provide a systematic meta-analysis of strongly CPL-active Eu^{III}, Tb^{III}, Sm^{III}, Yb^{III}, Cm^{III}, Dy^{III} and Cr^{III} complexes, discussing the suitability of their photophysical properties and highlighting promising candidates. We conclude by providing key recommendations for the development and advancement of the field.

[H1] Introduction

Counterfeiting is detrimental to commerce, health and society more broadly. Counterfeit medicines are estimated to cause on the order of a million human deaths annually and international trade in counterfeit goods is projected to be worth ~\$1 trillion USD by 2022¹ with the proceeds linked to criminal activities.² A plethora of noticeable and concealed anti-counterfeiting measures and technologies have been developed to combat counterfeiting, including physical measures such as tamper-proof labels, tracking labels, near-field communication tags, and security threads. However, many anti-counterfeiting technologies read extrinsic labels or intrinsic chemical information using non-ionising optical techniques.^{3–}

20

Perhaps the most well-known class of anti-counterfeiting labels are luminescent security inks, which are commonly applied to bank notes, drivers licences and passports (Fig. 1a–c).^{9,11,21–23} The luminescent security dyes incorporated in these inks have many essential features. They should be invisible to the naked eye and luminesce brightly when excited with UV-A light, for example the 365 nm light-emitting diodes (LED) used in commercial document scanners.²⁴ The security dyes should be readily soluble for use as inks and retain their necessary properties on deposition. They must be resistant toward fading and photobleaching and be thermally robust to survive conditions such as the relatively high temperatures (often excess of 150 °C) required for document lamination.^{25–27} Crucially, it must be viable to manufacture security inks on industrial scales for widespread application.^{18,28} Beyond these prerequisites, advanced luminescent security inks may incorporate further security features. For example, multiplexed emission via differential excitation and time-gated detection (Fig. 1d–f).^{11,18,21,22,27} Multi-scale and multi-modal authentication/read-outs are also desirable, for example by enabling at-a-glance inspection whilst also incorporating patterning or spectral features that can only be confirmed using specialist spectroscopic or microscopic instrumentation. Security can be further enhanced by incorporating features that cannot be copied because they result from a

random process (PUFs) that affords a truly unique label/tag giving a unique authentication readout.^{11,12} In general, the more features a luminescent security ink can incorporate, the more secure it will be.

This Review examines the application of a new advanced security ink feature: a hidden chiral fingerprint encoded into luminescence by circularly polarised luminescence (CPL). CPL is the lesser-known emission equivalent of circular dichroism and is generated from intrinsic chirality of luminescent molecules/complexes. It is not possible to replicate CPL without advanced chiral chemistry expertise and methods such as chiral high-performance liquid chromatography to isolate single enantiomers of dyes.²⁷ Additionally, CPL can serve as an additional layer on a document that cannot be detected without specialist optical read-out equipment. Many classes of chiral molecules emit CPL to varying degrees (Table 1) but in this Review we propose that molecular lanthanide complexes are uniquely suited to serve as CPL-active advanced security inks.

[H2] Lanthanide luminescence and security inks

Lanthanides ($Z = 57-71$) are f -block elements that exhibit many exceptional and advantageous luminescence properties that make them outstanding candidates for CPL-active security inks (Table 1). Despite being referred to as ‘rare earth’ elements, lanthanides are not particularly rare in the Earth’s crust, and are used commercially, for example as catalysts, magnets, magnetic resonance imaging contrast agents and as phosphors for displays.^{27,29} The exceptional luminescence properties of lanthanides arise from their partially filled $4f$ shell lying at lower energy than their $5s$ and $5p$ shells, which shield the $4f$ shell from the ligand environment.³⁰⁻³² This is the basis for the ‘lanthanide contraction’, whereby increases in Z are accompanied by population of the $4f$ shell. But these additional electrons do not effectively shield the $6s$ shell electrons from the positive charge of the nucleus, such that the atomic radius of the lanthanides diminishes with increasing atomic number.³⁰ The shielding of the $4f$ electrons has profound effects on the optical spectra of lanthanides. When excited, typically with ultraviolet light, lanthanides exhibit characteristically narrow and well-constrained ‘line-like’ emission bands and emission lifetimes in the ms regime. These bands are assigned to electric-dipole-forbidden $4f \rightarrow 4f$ emissive transitions between orbitals that experience the ligand field only weakly, with splittings being on the order of 100 cm^{-1} .³³ The forbidden nature of the $f \rightarrow f$ transitions results in the lowest energy excited states of lanthanides having long natural lifetimes.³⁴ Interested readers can learn more about Eu^{III} emission spectra elsewhere.³¹ We emphasize here that the influence of ligands can lower the symmetry around a Ln^{III} ion such that the Laporte-forbidden $4f \rightarrow 4f$ transitions become partly allowed and even ‘hypersensitive’ to the co-ordination of the lanthanide ion. Therefore, lanthanide luminescence can be harnessed for chemical sensing applications.³⁵

Lanthanide complexes have other advantages over organic dyes in security ink applications. Ln^{III} complexes exhibit line-like emission with large pseudo-Stokes shifts, minimal self-quenching and resistance to photobleaching.³⁶ Of particular interest here, Ln^{III} complexes can efficiently undergo circularly polarised luminescence (Table 1) in visible and near infrared (NIR) wavebands, with each lanthanide displaying a characteristic emission spectrum. Eu^{III} exhibits overall intense red emission, Tb^{III} exhibits overall intense green emission, Sm^{III} exhibits a less intense overall purple emission and Dy^{III} exhibits less intense blue/green emission.^{11,37-40} In contrast, Yb^{III} and Nd^{III} complexes emit in the NIR region.^{41,42} The key energy levels involved in the emission of circularly polarised photons from Ln^{III} are summarized in Dieke diagrams, one of which is available for Eu^{III} , Tb^{III} , Sm^{III} , Dy^{III} and Yb^{III} complexes,⁴³ with a more comprehensive diagram covering all trivalent lanthanides.⁴⁴ Additionally, lanthanide

emission can be multiplexed with other fluorophores to achieve advanced colour selection properties. For example, spatial multiplexing of red, green and blue emission creates full-colour luminescent images only visible under appropriate illumination.¹ Time-gated detection can also be used to distinguish long-lived lanthanide emission (ms lifetime) from short-lived organic fluorophores (ns lifetimes), enabling time-resolved colour multiplexing and separation (Fig. 1d–f).

As we noted above, free Ln^{III} ions have very low molar extinction coefficients for direct excitation because their centrosymmetric nature precludes the symmetry-forbidden $4f-4f$ transitions. To meet the demands of security inks, we must prepare suitable metal–organic complexes and either isolate them before making the ink or generating them in situ on the substrate. Suitable ligands can serve as efficient antennae to sensitize the $4f-4f$ transitions and protect Ln^{III} against exogenous binders.^{24,45–47} This principle can be extended to incorporate Ln^{III} into macromolecular systems such as nanoparticles, nanofibres or polymers to endow them with favourable properties.^{11,48–51} In particular, we now describe how incorporating Ln^{III} into chiral complexes can induce CPL as a ‘hidden fingerprint’ — an advanced security feature in the already distinct total luminescence spectra of Ln^{III} (Fig. 2).

[H2] Physics of circularly polarised light

Circularly polarised photons can be generated by various means, including by emission from diverse chiral molecules (Table 1) or devices such as LEDs, organic LEDs (OLEDs), plasmonic nano-antennas, liquid crystals and lasers.^{52–55} In the framework of quantum theory, left handed circularly polarised and right handed circularly-polarised photons correspond to spin angular momentum of $+h/2\pi$ and $-h/2\pi$ respectively.^{56–58} Building on this, linearly polarised light can be thought of as consisting of an equal number of left and right circularly polarised photons.⁵⁸ Elliptical polarisation can be thought of as various intermediate combinations of circularly polarised and/or linearly polarised photons.⁵⁹

Circularly polarised light can be more simply understood by considering a linearly polarised light wave, whose the resultant electric field vector arises from two orthogonal and equal magnitude x and y components of a transverse electromagnetic wave propagating along the z axis.⁶⁰ When the x and y components are in-phase, the resultant electric field vector oscillates in a single plane at 45° to both the x and y components, resulting in linear polarisation (Fig. 2a). The phases of the x and y components of the electric field can be manipulated by use of birefringent wave plates.⁶¹ Wave plates have a fast axis and a slow axis, orientated at 90° to each other. In the case of a vertical linearly polarised light wave incident at 45° to the fast axis of a half-wave plate (HWP), the phase of the slow axis of the light wave will be retarded by 180° ($\lambda/2$), resulting in the wave now becoming horizontally linearly polarised. Similarly, a quarter wave plate (QWP) can be used to convert linearly polarised light into circularly polarised light by retarding the phase of the slow axis by 90° ($\lambda/4$).⁶² The resultant overall electric field rotates, effectively tracing out a helical pattern as the wave propagates (Fig. 2a). Left and right circular polarisation refers to the direction of rotation of the resultant electric field vector as the wave propagates.

[H2] Perceiving CPL at a glance

A limited number of animals can perceive circularly polarised light. For example, stomatopod crustaceans and scarab beetles have evolved the exceptional ability to see circularly polarised light, which they use to covertly signal to members of their own species.^{63–66} Despite some residual sensitivity to polarised light (manifesting as visual phenomenon such as Haidinger’s brushes), the unaided human eye cannot distinguish images formed from light of different

polarisation states.^{67,68} Therefore external visual aids incorporating appropriate optical components (bandpass filter, QWP and linear polariser) are needed for humans to inspect CPL-active security inks ‘at a glance’. A bandpass filter enables selection of a wavelength range with the required circular polarisation properties. A QWP then converts left and right circularly polarised light into orthogonal linearly polarised light states, which are then selectively transmitted or blocked by an appropriately orientated linear polariser (Fig. 2b).

At the time of writing, circularly polarised light is most often perceived by members of the public when viewing 3D displays through specialist eyewear. In the context of 3D display technologies, two separate images are displayed: one rendered in left-handed circularly polarised luminescence (L-CPL) and one in right-handed circularly polarised luminescence (R-CPL). Each of these images can be selectively filtered by specialist 3D glasses incorporating a QWP and an appropriately orientated linear polariser in each lens to allow the viewer to perceive a 3D image.⁶² Although the performance of components in low-cost 3D glasses is poor relative to laboratory-standard materials, they are likely sufficient to distinguish between CPL emission states. Therefore, if adapted with a bandpass filter, such 3D glasses could likely be used for cheap and rapid at-a-glance verification of CPL-active security inks, such as on a banknote (Fig. 2c–e).

[H2] Applying CPL-active security inks

CPL-active security inks could be used in a variety of ways to create multi-layered security features required by end-user applications. We address them here in order of increasing complexity. The first case concerns a single enantiomer of a CPL-active complex applied as a homogeneous ink. This security ink would be invisible to the naked eye and under UV-A excitation would be indistinguishable from conventional Ln^{III} security inks (Fig. 1a). However, inspection with appropriate CPL-analysis equipment would reveal the CPL pattern for verification (Fig. 2c–e). Building on this, two enantiomers of the same CPL-active complex could be deployed as separate security inks to create multiplexed CPL-active patterning for inspection at a glance or with microscopy (Fig. 2c–e). Mixing enantiomers in various ratios could create a weighted CPL signal, analogous to blended whiskies.⁶⁹ More apparently, multi-colour CPL patterns could feature more than one lanthanide species, such as Tb^{III} complexes for green CPL and Eu^{III} complexes for red CPL. As a final layer of complexity, CPL-active security inks could be loaded into large nano- or micro-carriers such as nanoparticles to enable deployment in micro-scale unclonable patterning by stochastic processes.^{11,12,70,71}

[H2] Quantifying strength of CPL emission

The fraction of the total luminescence that is CPL is described in terms of the emission dissymmetry factor g_{em} (sometimes alternatively denoted g_{lum}):

$$g_{em} = \frac{2(I_{L-CPL} - I_{R-CPL})}{(I_{L-CPL} + I_{R-CPL})} \text{ (Equation 1)}$$

Where I_{L-CPL} and I_{R-CPL} are the intensities of L-CPL and R-CPL emission at a given wavelength, respectively. In the limiting cases, $g_{em} = 2$ indicates 100% L-CPL emission, $g_{em} = -2$ indicates 100% R-CPL emission and $g_{em} = 0$ indicates net zero circular polarisation. We can compute g_{em} values for an entire spectrum but g_{em} values are prone to amplifying noise (primarily arising from the CPL spectrum), such we generally report them at specific wavelengths/emission bands of interest.^{43,72} In brief, for lanthanide complexes, high g_{em} values in each well-defined ΔJ emission band arise from electronic transitions that are magnetic-dipole-allowed (mJ to mJ) and electric-dipole forbidden.^{43,73} However, it is

important to note that transitions may have a high g_{em} value yet be poorly emissive; this makes it more difficult to measure CPL in the rapid manner required for security inks. Therefore, it is important to quantify both the overall emission brightness and strength of CPL emission when assessing complexes for CPL-active security inks. To this end, it is first necessary to quantify circularly polarised brightness, CPB .^{29,74} First, total emission brightness (B) is defined as:

$$B = \varepsilon_{\lambda} \Phi \text{ (Equation 2)}$$

Where ε_{λ} is the molar extinction coefficient of a complex at a given emission band, and Φ is the overall quantum yield of emission from a complex. CPB is defined according to:

$$CPB = B \frac{g_{em}}{2} = \varepsilon_{\lambda} \Phi \frac{g_{em}}{2} \text{ (Equation 3)}$$

The units of CPB are $M^{-1}cm^{-1}$. If we consider CPB of an individual emission band we must introduce the branching ratio β_i , the proportion of total emission contributed by an individual transition i :

$$\beta_i = \frac{I_i}{\sum_j I_j} \text{ (Equation 4)}$$

Where $\sum_j I_j$ is the total emission across the total number (j) of transitions and I_i is the proportional emission of transition i . Therefore, we define CPB for a single transition, CPB_i , as:

$$CPB_i = \beta_i B \frac{g_{em}}{2} \text{ (Equation 5)}$$

CPB_i has been alternatively denoted as B_{CP} , and is reported in units of $M^{-1}cm^{-1}$. Herein, we use CPB — more specifically, CPB_i — as the primary metric to assess candidate complexes for application in CPL-active security inks. CPB_i values for many different CPL-active complexes were recently estimated.⁷⁴ For convenience, the averages of these CPB_i estimates for various classes of complexes are collated in Table 1.

In general, lanthanide complexes afford excellent CPB_i and g_{em} values. Indeed, a recently reported CPL-active Eu^{III} complex $([(Eu_4L_4)((R/S)\text{-BINAPO})_4])$ (BINAPO = 2,2' bis(diphenylphosphoryl)-1,1'-binaphthyl) gives rise to a $\Delta J = 1$ emission band with CPB_i 3000 $M^{-1}cm^{-1}$ — the highest of any class of CPL-emitter to-date.⁷⁵ The strongest CPL emission to-date in terms of g_{em} values arises from monomeric ($g_{em} \sim |1.38\text{-}1.41|$, $\Delta J = 1$) and helical aggregates ($g_{em} = |1.45|$, $\Delta J = 1$) forms of $Cs\{Eu[(+,-)\text{-hfbc}]_4\}$ ($hfbc^- = 3\text{-heptafluorobutyryl camphorate}$) (see Fig. 3b).^{51,76,77} CPL emission from the enantiomers of the latter complex was notably differentiable to the eye at a glance using external visual aids as discussed above,⁵¹ yet the monomeric form of $Cs\{Eu[(+,-)\text{-hfbc}]_4\}$ offers a relatively low CPB_i of only $\sim 51 M^{-1}cm^{-1}$, which is well below the average (286 $M^{-1}cm^{-1}$) and median (87 $M^{-1}cm^{-1}$) for Eu^{III} complexes.^{74,77}

CPB_i is generally maximised for an emission band (or often individual transitions thereof) that has a high molar extinction coefficient, high emission quantum yield and a modest g_{em} value (eq. 5). Unfortunately, bands that have high g_{em} values are not generally associated with high quantum efficiencies, so there is a trade-off between g_{em} and CPB_i . Whilst both g_{em} and CPB_i are very useful metrics, they should not be a blunt comparison tool. Rather, the collective

photophysical and CPL properties of a complex should be considered in the context of a desired application. A complex with a large g_{em} value will maximise contrast for enantioselective CPL imaging,^{51,78,79} whereas a complex with high CPB_i can provide large quantities of circularly polarised photons, ideal for high-throughput rapid CPL verification, such as screening bank notes.

[H1] Advances in CPL spectroscopy and imaging

Although many CPL-active complexes have been developed over the past 50 years, the technology used to measure CPL has been somewhat stagnant. In this section, we discuss recent breakthroughs in CPL measurement technology that enable rapid, high-throughput, security-ink verification.

[H2] Legacy PEM-SM CPL spectrometers

The CPL spectrometers used to collect data for studies reported from the 1970s through to 2020 operate according to the same fundamentals. These legacy instruments are slow and require ~1 hour to scan a typical lanthanide luminescence spectrum. They are bulky, unadaptable and expensive to build, maintain or purchase (>£100,000).⁷² They feature a photo-elastic modulator (PEM) and lock-in amplifier to convert CP light to linearly polarised light for analysis, as well as a scanning monochromator (SM) to spectrally filter light for analysis (Fig. 4a). We thus refer to such instruments as PEM-SM-CPL spectrometers.⁸⁰

Acquiring data with a PEM-SM-CPL spectrometer is slow because SMs scan wavelengths in a stepwise fashion and CPL analysis components lower light throughput, which is particularly detrimental because of the inherently weak nature of CPL relative to total emission intensity. For example, our custom-built PEM-SM-CPL spectrometer requires ~45 minutes to acquire a scan of a typical Eu^{III} complex with default scan settings (150 nm spectral window, 1 ms dwell time / 0.5 nm increments, 5 spectral accumulations).⁷² Time-gated CPL measurement has been achieved with some PEM-SM-CPL spectrometers,^{81–85} but only over a limited wavelength window, with a poor signal-to-noise ratio (SNR) and substantially increased scan times.^{86,87} Given that time-gated measurements are already challenging over a small wavelength window we can safely say that time-gated full-spectrum CPL measurements are impractical with PEM-SM-CPL spectrometers.

Despite the severe drawbacks of PEM-SM-CPL spectrometers, they are likely to remain used in academic research because these tried-and-tested instruments and represent a large monetary investment. After all, given enough time they can measure very weak CPL spectra, provided the sample of interest is robust and not susceptible to photobleaching. However, PEM-SM-CPL spectrometers are clearly impractical for high-throughput security-ink applications.

[H2] Next-generation rapid-CPL spectrometers

Recently innovated next-generation CPL spectrometers offer superior performance over PEM-SM-CPL spectrometers in terms of cost, flexibility/modularity and sub-second time-gated full spectrum CPL acquisition. Whilst next-generation CPL spectrometers are not yet commercially available, the components required can be readily sourced, making them affordable to construct. Further, there is scope for further cost reduction and miniaturisation. Therefore, the sub-second measurement capabilities of next-generation CPL spectrometers make them ideal for high-throughput verification of CPL-active security inks.

The first next-generation rapid CPL spectrometer was reported in early 2020 (Fig. 4b).^{72,88} It uses linear solid-state (SS) charge-coupled device (CCD) detectors and is therefore referred to

as a SS-CPL spectrometer. At the heart of the SS-CPL spectrometer is a simple CPL analysis system. First, a QWP converts L-CPL and R-CPL light into orthogonal linear polarisations, which are then spatially separated into two detection arms by a beam-splitter. The light in each arm is analysed by a linear polariser in a high-precision motorised rotation mount and is subsequently measured in as little as 10 ms by a linear CCD spectrometer operating between 400 and 800 nm. Time-gating is achieved simply by delaying detection with respect to excitation pulses. This SS-CPL spectrometer was benchmarked against an established PEM-SM-CPL spectrometer, demonstrating improved SNR with perfect agreement to well-established g_{em} values of Eu^{III} complexes measured⁷²

A second next-generation CPL spectrometer was reported later in 2020.⁸⁹ This spectrometer was designed to detect NIR emission and is therefore referred herein as a NIR-SS-CPL spectrometer. The NIR-SS-CPL spectrometer is based on a fundamentally similar design to the SS-CPL spectrometer, in that CPL is converted into orthogonal linear polarised states by a QWP and a polarising beam-splitter subsequently converts/analyses L-CPL and R-CPL into orthogonal linear polarisation states. These states are then spatially split and fibre optics deliver them to a SM for spectral filtering and subsequent detection with a NIR CCD or NIR photomultiplier tube. Due to the SM, spectral acquisition takes ~ 1 s.⁸⁹ Full operational details of the NIR-SS-CPL spectrometer, including calibration, are not available at the time of writing and validation of the NIR-SS-CPL spectrometer has not yet been published. This spectrometer has been used to measure CPL emission from a helical Yb^{III} complex. Overall, next-generation rapid CPL spectrometers are proliferating. The lower limits of their sensitivity are yet to be established, but they are more than adequate for measuring and verifying CPL emission from Ln^{III} complexes that have g_{em} on the order of 10^{-1} .

[H2] CPL-contrast enantioselective imaging

A demonstration of enantioselective CPL contrast imaging came in 2016 with the adaptation of an epifluorescence microscope for CPL analysis.²⁷ The necessary modifications were relatively simple: retrofitting the detection pathway with a QWP and a selector for two orthogonally orientated linear polarisers. This set-up was used to examine enantiomers of a complex with strong CPL emission EuL^1 ($\text{Eu}[1,4,7\text{-Tris}(\{4\text{-}[2\text{-}(4\text{-methoxy-2-methylphenyl})\text{ethynyl}]\text{-6-[carboxy(phenyl)phosphoryl]pyridin-2-yl}\}\text{methyl})\text{-1,4,7-triazacyclononane}]$ see Fig. 3e) ($\Delta J = 1$ $g_{em} = \pm 0.11$; $CPB_i = 117 \text{ M}^{-1}\text{cm}^{-1}$) and afforded an enantioselective contrast ratio of 3.4:1 — that is L-CPL features were 3.4 times brighter than R-CPL features when selected for and vice-versa.²⁷ The study also included a proposal on how to adapt a confocal microscope for enantioselective CPL-contrast imaging. Later work demonstrated the utility of enantioselective CPL microscopy to image the enantioselective distribution of chiral Eu^{III} complexes in living cells.⁹⁰ For security ink applications, such microscopes could be used to analyse micro-scale CPL patterning.

A recent study of enantioselective CPL imaging on a glass substrate used a simple CPL imaging set-up to select for CPL emission from Eu^{III} complexes embedded onto a glass surface.⁷⁸ The complex (see Fig. 3g) was generated from $\{\text{Eu}[(+,-)\text{-facam}]_3\}$ ($\text{facam}^- = 3\text{-}(\text{trifluoroacetyl})\text{camphorato}$, a β -diketonato ligand) and two molar equivalents of the glass-forming agent tmpo (tmpo = tris(2,6-dimethoxyphenyl)phosphine oxide), was excited with UV-A light (365 nm), exhibited a strong enantiomeric contrast ($g_{em} = \pm 1.2$, $\Delta J = 1$), and a quantum yield of 13%. The individual enantiomers were separately deposited on a glass substrate and the solvent evaporated to leave a sun-and-moon pattern by a casting process to create ‘lumino-glass’. When L-CPL was selected, the sun was brightly visible whilst the moon was dim. This pattern was reversed for R-CPL (Fig. 2e). Although an enantioselective contrast ratio was not

reported, this study is the best example of macro-scale enantiomeric contrast imaging to date and clearly demonstrates the potential of advanced CPL-active security inks.⁷⁸ It is not a large leap to envision such techniques being used for at-a-glance authentication of products such as high-performance glass (for security or display technologies), or to manufacture visually impressive luxury drink bottles.³ Already, human observers can differentiate L-CPL and R-CPL at a glance from solid Cs{Eu[(+,-)-hfbc]₄} because of the strong signal from its ⁵D₀ → ⁷F₁ ($\Delta J = 1$) transition ($g_{em} \sim 1.38-1.41$, $CPB_i \sim 50 \text{ M}^{-1}\text{cm}^{-1}$).^{51 51} All this requires is passing the emitted light through a bandpass filter, QWP and linear polarizer, a set-up amenable to rapid verification of CPL-active security inks.

Despite their aforementioned technological limitations, PEMs have been used for quantitative CPL-mapping microscopy, although this does require long scan times. Such microscopes have been used to examine dyes,^{91,92} crystals,⁹³ thin films of helical fibres,⁹⁴ polymer aggregates⁹⁵ and interactions between Eu^{III} complexes and amino acids within agar gel substrates.⁹⁶ PEM CPL microscopes certainly have utility as research tools but their slow scan rates precluded their use to validate security inks.

Overall, recent years have seen enantioselective CPL imaging with the aided human eye, with a simple camera system and with an epifluorescence microscope. Systems to enantioselectively image CPL-active security inks are likely to be adapted from conventional imaging systems by adding suitable bandpass filters, QWPs and linear polariser elements. These should enable convenient enantioselective CPL-contrast imaging.

[H1] Meta-analysis CPL-active Ln^{III} complexes

The literature was searched for peer-reviewed publications reporting CPL-active lanthanide complexes prior to 31st May 2020. Complexes were considered if they exhibited CPL with $g_{em} \geq 0.05$, excluding CPL from electroluminescence or circularly polarised excitation. Complete details of our methodology are provided in the Supporting Information, with key photophysical characteristics presented in Table 1. We now survey the emissive complexes, organizing them according to the Ln^{III} metal ions.

[H2] Eu^{III} complexes

Eu^{III} complexes features a non-degenerate emissive ⁵D₀ state, which gives rise to relatively simple and distinct emission spectra. The form and relative intensity of the ⁷F_{*n*} → ⁵D₀ ($n = 0-4$) transitions vary with respect to the speciation and symmetry of the Eu^{III} centre, with the $\Delta J = 2$ and $\Delta J = 4$ bands showing particular sensitivity to the local coordination environment. Meta-analysis reveals striking differences with regards to maximum g_{em} values for the four main emission bands of Eu^{III} that have not clearly been reported before (Fig. 5a). The Eu^{III} ⁵D₀ → ⁷F₁ ($\Delta J = 1$) band has the potential to generate exceptional g_{em} values as high as $\sim |1.4|$ because the oscillator strength of the magnetic-dipole-allowed $\Delta J = 1$ band is generally considered to be independent of the ligand environment. In contrast, the $\Delta J = 2$ and $\Delta J = 4$ bands are electric-dipole-allowed and are hypersensitive to ligand perturbation with their intensities being proportional to the square of the ligand dipolar polarizabilities. Electric-quadrupole-allowed transitions (⁵D₀ → ⁷F₂ and ⁵D₀ → ⁷F₄) gain electric dipole strength through a quadrupole (on the Ln^{III} ion)-induced dipole (ligand donor group) coupling mechanism. The induced dipoles on the ligands result from direct coupling to the electric dipole components of the radiation field. Thus, the transition dipole moment of $4f \rightarrow 4f$ transitions is directly affected by ligand dipolar polarizabilities and to the anisotropies of these polarizabilities.⁹⁷⁻⁹⁹

Our meta-analysis indicates that the $\Delta J = 2$ and $\Delta J = 4$ bands of Eu^{III} complexes are limited to $g_{\text{em}} < \sim 0.3$ and $g_{\text{em}} < \sim 0.4$, respectively (Fig. 5a). The $\Delta J = 3$ band, which is magnetic-dipole-allowed and electric-dipole-forbidden, has a potential to yield moderately strong g_{em} values up to $\sim |0.7|$ but is by far the weakest in terms of relative emission intensity, limiting its CPB_i . Therefore, the ${}^5\text{D}_0 \rightarrow {}^7\text{F}_1$ and ${}^5\text{D}_0 \rightarrow {}^7\text{F}_2$ bands are most likely to give rise to the high CPB_i values necessary for CPL-active security-ink applications.

To our knowledge, only one report describes image contrast of a CPL-active Eu^{III} (EuL^I) complex impregnated onto a paper substrate (see Fig. 3e).²⁷ The complex chosen has $\Delta J = 1$ transitions with a good quantum yield ($\sim 50\%$) and modest CPL ($g_{\text{em}} = \pm 0.15$ in solution and ± 0.10 on paper) to give a useful overall CPB_i of $134 \text{ M}^{-1}\text{cm}^{-1}$. This study was a proof-of-concept for the wider field, with later work demonstrating enantioselective imaging of CPL-active lumino glass (see Fig. 2e and 3g).⁷⁸ We now instead move on to describe examples based on their solution photophysical properties.

In solution, several Eu^{III} complexes exhibit the desired photophysical properties for CPL-active security inks, such as UV-A excitation and high CPB_i values. The tetrahedral Eu^{III} complexes $\Delta\Delta\Delta\Delta$ -/ $\Lambda\Lambda\Lambda\Lambda$ - $[(\text{Eu}_4\text{L}_4)(\text{DPEPO})_4]$ (DPEPO = bis[2-(diphenylphosphino)phenyl] ether dioxide (see Fig. 3d); $\text{H}_3\text{L} = 4,4',4''$ -tris(4,4,4-trifluoro-1,3-dioxobutyl)triphenylamine, a tris(β -diketone)) and $[(\text{Eu}_4\text{L}_4)((R/S)\text{-BINAPO})_4]$ (BINAPO = 2,2'-bis(diphenylphosphoryl)-1,1'-binaphthyl) have $\Delta J = 1$ transitions that afford CPB_i of $1122 \text{ M}^{-1}\text{cm}^{-1}$ and $3240 \text{ M}^{-1}\text{cm}^{-1}$, respectively, the highest values of any known complex.⁷⁵ These CPB_i values are an order of magnitude greater than the average $\Delta J = 1$ CPB_i for Eu^{III} complexes ($294 \text{ M}^{-1}\text{cm}^{-1}$).⁷⁴ These excellent CPB_i values are a result of excellent quantum yields ($\sim 70/80\%$), a high molar extinction coefficient for UV-A (395 nm) and modest g_{em} values. Rather unusually, the characteristic red Eu^{III} luminescence of this complex was apparent even under standard room light illumination. Due to their excellent CPB_i properties, these complexes should be investigated for advanced security ink applications as a priority.

A recently developed CPL calibration complex $\{\text{Eu}[(4\text{-methoxyphenyl)alkynyl-bpepc}]_3\}\text{Cl}_3$, (see Fig. 3c) — an analogue of $[\text{Eu}(\text{bpepc})_3]\text{Cl}_3$ (bpepc = N,N' -bis(1-phenylethyl)-2,6-pyridinedicarboxamide),^{100,101} with additional (4-methoxyphenyl)alkynyl substituent on the pyridine 4-positions — has a very good CPB_i of $102 \text{ M}^{-1}\text{cm}^{-1}$ and $212 \text{ M}^{-1}\text{cm}^{-1}$ ($\Delta J = 1$ and 2, respectively) when excited at 365 nm. This arises from a more modest quantum yield but excellent excitation and moderately strong CPL emission ($g_{\text{em}} \pm 0.25$, ${}^5\text{D}_0 \rightarrow {}^7\text{F}_1$; $g_{\text{em}} \pm 0.10$, ${}^5\text{D}_0 \rightarrow {}^7\text{F}_2$).¹⁰² Overall, further work is required to ascertain whether $\{\text{Eu}[(4\text{-methoxyphenyl)alkynyl-bpepc}]_3\}\text{Cl}_3$ will be viable as a CPL-active security ink on paper substrates and more generally, if complexes that undergo dynamic ligand exchange are viable on paper substrates.

$\text{Cs}\{\text{Eu}[(+,-)\text{-hfbc}]_4\}$ (see Fig. 3b) is a prominent candidate for enantioselective CPL contrast imaging because of its exceptionally strong CPL properties as both a monomer and a helical aggregate.^{51,76,77} In monomeric form, $\text{Cs}\{\text{Eu}[(+,-)\text{-hfbc}]_4\}$ exhibits ($g_{\text{em}} \geq |1.38\text{-}1.41|$, ${}^5\text{D}_0 \rightarrow {}^7\text{F}_1$, 0.6% quantum yield) and favourable UV-A excitation (350–370 nm).^{74,76} By controlling the concentration of the $\text{Cs}\{\text{Eu}[(+,-)\text{-hfbc}]_4\}$ monomeric building blocks and a chiral inhibitor $\text{Eu}[(+,-)\text{-hfbc}]_3$ (inhibitor), these monomers $\text{Cs}\{\text{Eu}[(+,-)\text{-hfbc}]_4\}$ can be polymerised into a higher-order helical aggregate form with a typical length of several microns with improved photophysical properties ($g_{\text{em}} \geq |1.45|$, ${}^5\text{D}_0 \rightarrow {}^7\text{F}_1$, 1.0% quantum yield). CPL emission of opposite enantiomers of helical aggregates of $\text{Cs}\{\text{Eu}[(+,-)\text{-hfbc}]_4\}$ was so strong as to be differentiable by the aided human eye.⁵¹ However, regardless of the aggregation state or cation

used, $\{\text{Eu}[(+,-)\text{-hfbc}]_4\}^-$ exhibits a relatively poor quantum yield¹⁰³ that limits its estimated CPB_i values to $50.7 \text{ M}^{-1}\text{cm}^{-1}$ ($\Delta J = 1$) and $59.1 \text{ M}^{-1}\text{cm}^{-1}$ ($\Delta J = 2$).⁷⁴ Thus, further testing is required to ascertain the utility of $\text{Cs}\{\text{Eu}[(+,-)\text{-hfbc}]_4\}$ as a high-contrast enantioselective CPL-active security ink.

Other promising Eu^{III} complexes combine favourable photophysical properties to give CPB_i values on the order of $100 \text{ M}^{-1}\text{cm}^{-1}$ with UV-A excitation.^{104,105} CPB or CPB_i values have not been estimated for many of these and we anticipate that, for example, quadruple helicates $\Delta\Delta/\Lambda\Lambda\text{-}(\text{HNEt}_3)_2[\text{Eu}_2\text{L}_4]$ (where L^{2-} is a chiral bis(β -diketonato) ligand) with exceptional photophysical properties may afford exceptionally large CPB_i values.¹⁰⁶ The NMR-shift reagent $\{\text{Eu}[(+,-)\text{-facam}]_3\}$ (see Fig. 3a) warrants consideration due to its strong CPL emission ($g_{\text{em}} \sim -0.8$, ${}^5\text{D}_0 \rightarrow {}^7\text{F}_1$) and commercial availability. However, only a single enantiomer of this complex is commercially available and its CPB_i is likely limited by a somewhat low brightness.^{72,80,107} Other designs may be viable,^{108–110} one example being the heptanuclear Eu^{III} complex salt $\{\text{Eu}[\text{C}[\text{Eu}((R/S)\text{-Phbipox})_2]_6](\text{OTf})_9$ ($\text{Phbipox}^- = 6'-(4\text{-phenyloxazolin-2-yl})-2,2'$ -bipyridine-6-carboxylato), which features a tetradentate ligand.¹¹¹

In general, the CPL properties of Eu^{III} complexes have been well studied and numerous examples have potential to be incorporated into CPL-active security inks. However, published studies typically lack the experimental tests necessary. Indeed, as we noted above, only a single CPL-active Eu^{III} species has been measured on a paper substrate.²⁷ Paper deposition tests are important because it shows that a complex can be resistant to ligand dissociation and/or solvent effects that would otherwise dramatically alter both total and CPL luminescence.^{102,112} Nevertheless, more recently developed tetrahedral Eu^{III}_4 complexes afford CPB_i of $\sim 1000\text{--}3000 \text{ M}^{-1}\text{cm}^{-1}$ — values an order of magnitude greater than those of any other Eu^{III} complex.^{74,75} Although providing fewer overall circularly polarised photons, the classic salt $\text{Cs}\{\text{Eu}[(+,-)\text{-hfbc}]_4\}$ could provide exceptionally high enantioselective contrast.^{51,74} Lastly, there is a clear potential for red Eu^{III} CPL-active security inks that needs to be developed.

[H2] Tb^{III} complexes

Tb^{III} complexes give rise to a characteristic green luminescence and typically require higher energy excitation ($\lambda_{\text{ex}} < 350 \text{ nm}$) than Eu^{III} complexes because the latter have more accessible triplet states ($20,500 \text{ cm}^{-1}$ vs $17,200 \text{ cm}^{-1}$). The studies that we considered all reported Tb^{III} emission in solution and g_{em} values for Tb^{III} species are more limited than those for Eu^{III} and Sm^{III} complexes (Fig. 5b), perhaps because Tb^{III} is less sensitive to its coordination environment.²⁰ CPB_i values have only been reported for six Tb^{III} complexes, four of which exhibit relatively low g_{em} values and modest quantum yields. Yet, under the right conditions, Tb^{III} complexes can provide very useful CPB_i values in excess of $100 \text{ M}^{-1}\text{cm}^{-1}$.⁷⁴

There are several challenges in developing Tb^{III} complexes as CPL-active security inks and choosing an appropriate excitation wavelength is vital. Thus, $[\text{Tb}(\text{HL}^2)]$ (where (L^2) is an $(\text{O}_8)^{4-}$ -donor ligand, see Fig. 3f) can be excited at UV-A wavebands (350 nm), with very good quantum yields (57%) and modest-to-weak CPL emission ($g_{\text{em}} = 0.08$ at 545.8 nm).¹¹³ CPB_i for this complex was estimated to be $307 \text{ M}^{-1}\text{cm}^{-1}$ when excited in the UV-B region ($\lambda_{\text{ex}} = 303 \text{ nm}$).⁷⁴ Estimation of CPB_i at wavelengths in the UV-A would be useful for assessing the utility of $[\text{Tb}(\text{HL})]$. Other Tb^{III} complexes require higher energy excitation in the UV-B or UV-C ranges, rendering them unsuitable/impractical for security ink applications.^{74,114–116} Aside from excitation wavelength, the choice of solvent may also effect total emission and CPL emission in solution.¹¹⁷ An important and somewhat detrimental feature of Tb^{III} CPL is that multiple CPL sign inversions of individual electronic transitions within emission bands is common and

may reduce CPB_i for otherwise promising complexes.^{40,118–120} Another notable complex is $[\text{TbL}^3]^+$ (L^3 is an $(\text{O}_8)^{4-}$ -donor ligand), which is UV-A excitable (350 or 373 nm) and combines very good quantum yields (63%) with weak CPL emission ($g_{\text{em}} \pm 0.04$), leading to an estimated CPB_i of $195 \text{ M}^{-1}\text{cm}^{-1}$ ($\lambda_{\text{ex}} = 350 \text{ nm}$).^{39,74} Despite the aforementioned challenges, chiral Tb^{III} complexes may yet be viable as green CPL-active luminescent security inks.

[H2] Sm^{III} complexes

Complexes of Sm^{III} exhibit a characteristically purple luminescence.³⁹ We found ten studies reporting CPL-active Sm^{III} complexes in solution with no accompanying estimates of CPB or CPB_i . The range of g_{em} values reported are somewhat similar to those for species Eu^{III} (Fig. 5c). However, quantum yields for Sm^{III} species are universally very poor ($< 1\%$) and emission lifetimes are short ($\sim 30 \mu\text{s}$) relative to other lanthanide complexes.

$\text{Cs}\{\text{Sm}[(+,-)\text{-hfbc}]_4\}$ is the only reported Sm^{III} complex to give very strong CPL emission ($g_{\text{em}} \sim |1.15|$). Its CPL spectrum has many narrow emission peaks and several CPL sign inversions, which would limit its CPB_i values. Moreover, its excitation was reported at 338 nm, a short wavelength that is somewhat unfavourable but that may not preclude security ink applications.⁷⁷ Indeed, the Eu^{III} analogue $\text{Cs}\{\text{Eu}[(+,-)\text{-hfbc}]_4\}$ (see Fig. 3b) is excitable at 375 nm and exhibits a quantum yield of $\sim 1\%$.⁷⁶ However, the photophysical properties for the analogue $\text{Cs}\{\text{Sm}[(+,-)\text{-hfbc}]_4\}$ have not yet been established. Quantum yields have not been reported for several known CPL-active Sm^{III} complexes, which limits the preliminary assessment of their utility.^{104,121,122} and others require UV-B excitation.^{40,119}

It is fair to say that Sm^{III} complexes are not particularly well developed and often exhibit poor quantum efficiencies, which severely limits the CPB values achievable. However, there have been relatively few studies of CPL-active Sm^{III} complexes, so future work may yet improve excitation wavelengths, quantum yields and CPL emission properties in order to maximise CPB_i . Further, the relatively short luminescence lifetime (μs range) of Sm^{III} complexes could facilitate intermediate-range time-gated detection between organic fluorophores (ns lifetime range) and other lanthanides (ms lifetime range), thereby expanding options for time-gated colour dependence and spectral separation. At this early stage, $\text{Cs}\{\text{Sm}[(+,-)\text{-hfbc}]_4\}$ seems to be the main candidate of interest.⁷⁷ However, it seems unlikely that Sm^{III} complexes will be the first Ln^{III} complexes to be developed for CPL-active security inks, because Eu^{III} and Tb^{III} display more favourable and superior photophysical properties.

[H2] Dy^{III} complexes

Dy^{III} complexes emit from the blue to the NIR, with luminescence typically appearing as blue/green to the eye in solution.^{39,40,119} We found only four studies reporting CPL-active Dy^{III} complexes and CPB or CPB_i have not yet been quantified for any of them.^{39,40,74,118,119} Dy^{III} complexes exhibit emission lifetimes in the range of $\sim 10 \mu\text{s}$.

We mentioned above the complex $[\text{TbL}^3]^+$ of the dianionic O_8 -donor; this ligand has also been incorporated into a Dy^{III} complex that is excitable at a favourable UV-A wavelength (373 nm), albeit with very weak CPL ($g_{\text{em}} = 0.01$, 669 nm) from the ${}^4\text{F}_{9/2} \rightarrow {}^6\text{H}_{11/2}$ transition. Further, $[\text{DyL}^3]^+$ has a short emission lifetime of $17 \mu\text{s}$ and a poor quantum yield of 1.3% ,³⁹ such that it is likely to exhibit very low CPB . Stronger CPL has been reported from $[\text{DyL}^4]^{3+}$, a complex of the N_4O_4 donor L, a derivative of the macrocycle 1,4,7,10-tetraazacyclododecane bearing four amide groups. However, the ${}^4\text{F}_{9/2} \rightarrow {}^6\text{H}_{11/2}$ transition responsible for the CPL ($g_{\text{em}} = +0.35$ (657 nm), -0.41 (665 nm)) here is relatively dim and features several CPL sign inversions with the quantum yields being unknown.¹¹⁸ More newly-developed complexes have been excited

with unfavourable UV-B light and combine poor quantum yield (<0.5%) and weak-to-modest CPL properties.^{40,119}

Overall, CPL-active Dy^{III} complexes are in general not well developed. Whilst they could serve to provide blue/green luminescence with intermediate lifetimes (~10 μs), they are likely to be overlooked in favour of Tb^{III} and Eu^{III} complexes with better and more well-studied photophysical properties.

[H2] Yb^{III} complexes

Yb^{III} complexes typically exhibit luminescence in the NIR region between 900 and 1050 nm with weak-to-modest CPL emission. We found five studies reporting CPL from Yb^{III} complexes in solution.^{41,42,118,123,124} CPB_i values have been estimated for {Yb(TTA)₃(2,6-bis[2-(3-isopropylloxazoliny)]pyridine)} (HTTA = 1,1,1-trifluoro-4-(2-thiophenyl)-2,4-butanedione) and {Yb(TTA)₃(2,6-bis[2-(3-phenylloxazoliny)]pyridine)}.¹²³ These complexes can be excited with UV-A (365 nm) but the resulting quantum yields are very low (< 0.7%) and the CPL very weak ($g_{em} = \sim 0.02$). Indeed, CPB_i values for the isopropyl and phenyl-functionalized complexes (5.2 and 2.5 M⁻¹cm⁻¹, respectively; $\lambda_{ex} = 345$ nm)^{74,123} are two orders of magnitude lower than average CPB_i values of Eu^{III} and Tb^{III} complexes.

The chiral NMR shift reagent [Yb(+)(facam)₃]³⁺ can be excited with UV-A (360 nm) to yield relatively weak CPL ($g_{em} = -0.08$ at 975 nm), albeit with a very sharp and bright peak, which is promising in terms of maximizing CPB_i .⁴² The quantum efficiency of [Yb(+)(facam)₃]³⁺ has not been reported but this complex, like its counterpart [Eu((+,-)-facam)₃]³⁺ (see Fig. 3a), is commercially available. Commercial availability would be advantageous for security ink application and that alone may warrant further investigation into its photophysical properties.

[YbL]³⁺ (where L, is a N₄O₄ donor, a tetraamide derivative of 1,4,7,10-tetraazacyclododecane bearing substituents with (*S*)-stereocentres) can be excited in the UV-A region (380 nm) and emits weak to modest CPL ($g_{em} > |0.10|$ for the ²F_{5/2} → ²F_{7/2} transition). However, the CPL spectrum featured several sign inversions, limiting the potential CPB_i (quantum efficiency was not reported).⁴¹ Other complexes require UV-C excitation or have unclear photophysical properties.^{42,118,124}

We note that CPL-active Yb^{III} species are not well developed. At this preliminary stage, it seems that Yb^{III} complexes are unlikely to be developed as CPL-active security inks owing to their sub-par photophysical and CPL properties. They may only find use if there is a very strong requirement for NIR luminescence, but this also poses problems with the higher cost associated with the specialist NIR detectors required with such applications.

[H2] Other metal complexes

As with many of the lanthanides, Cr^{III} — sometimes referred to as ‘molecular ruby’ — can be relatively cheap and abundant,⁴³ and can afford complexes that exhibit CPL at NIR wavebands (> 700 nm). Cr^{III} complexes have been reported with favourable UV-A excitation, reasonable CPL strength, wide emission wavebands favourable to NIR CPL-contrast and good CPB_i (>100 M⁻¹cm⁻¹; Table 1).⁷⁴ Unfortunately, reported CPL-active Cr^{III} complexes are very sensitive to atmospheric gases, such as O₂^{125,126}; rendering them undesirable for routine security ink applications. Lastly, we note that Cm^{III} complexes can also be engineered to undergo CPL,¹²⁷ but their radioactive nature makes them unsuitable for security ink applications.

[H1] Conclusions

The scope and timing of this Review are inspired by advances in CPL measurement instrumentation, which since the mid-2010s have included the advent of rapid CPL spectroscopy and enantioselective CPL microscopy.^{27,72} Complementary developments in CPL-active complexes have also been reported. Key among these are Eu^{III} complexes with optimal photophysical properties — they emit unprecedented numbers of circularly polarised photons⁷⁵ making them ideal for high-throughput screening (Fig. 6). Further, processing strategies (for example, the formation of helical aggregates) have been developed to enhance CPL emission from already strong CPL emitters, making their CPL eye-differentiable at a glance.⁵¹ Therefore, we think of CPL-active complexes in terms of two broad classes: those which maximise enantiomeric contrast to give high g_{em} and those which maximise the number of circularly polarised photons for rapid and high SNR measurements.

Our meta-analysis and survey of the photophysical properties of CPL-active Ln^{III} complexes indicate that Eu^{III} complexes are the prime candidates for development as red CPL-active security inks, with Tb^{III} complexes also showing clear potential as green inks. At this stage there is not a compelling case for Sm^{III}, Dy^{III}, Yb^{III} or Cr^{III} security inks. However, Sm^{III}, Dy^{III}, Yb^{III} and Cr^{III} complexes are historically under-studied in comparison to Eu^{III} and Tb^{III} complexes. Therefore, some improvements in their photophysical properties may be made with future studies that could lead to niche applications. For example, Cr^{III} complexes could be deployed in applications where atmospheric sensitivity is of interest and Sm^{III} could provide μ s lifetime CPL for applications with an intermediate time-gate requirement.

Optimal photophysical and CPL properties are paramount for security inks. In this regard, we have highlighted some Eu^{III} and Tb^{III} complexes that should be investigated as red or green CPL-active security inks, namely $\Delta\Delta\Delta\Delta$ -/ $\Lambda\Lambda\Lambda\Lambda$ -[(Eu₄L₄)(DPEPO)₄],⁷⁵ [(Eu₄L₄)((*R/S*)-BINAPO)₄],⁷⁵ EuL^{1,27} {Eu[(4-methoxyphenyl)alkynyl-bpepc]₃}Cl₃,¹⁰² Cs{Eu[(+)-hfbc]₄},^{51,74,76} and TbHL.¹¹³ These complexes may not yet be optimal materials but are a good starting point for future investigations. Indeed, a number of Eu^{III} and Tb^{III} complexes could be viable as CPL-active security inks and a successful CPL-active complex must overcome a plethora of experimental hurdles before it can be incorporated into CPL-active security inks on substrates. The main purpose of the security ink should be considered when choosing the Ln^{III} complex. Does the application require rapid high-throughput CPL verification (where a high CPB_i value is of priority) or does the application require maximal enantioselective contrast (where a high g_{em} value is paramount)?

We recommend that candidate complexes be readily excitable with UV-A wavebands (for example, 365 nm) currently found in pre-existing commercial document scanners. Another practical consideration is that cost-effective optical bandpass filters with high transmission are not available for all waveband because they are typically made for specific applications such as common laser lines or fluorophore emission bands. A lack of an appropriate optical bandpass filter, especially for narrow transitions of Tb complexes, could hinder the adaption of pre-existing imaging/spectroscopy systems for CPL verification if not carefully considered. Further, when developing new complexes one should quantify both g_{em} and CPB_i because these metrics help objective comparisons. As we have seen, photophysical and CPL properties can be sensitive to solvents and atmosphere, such that different conditions should be investigated for solution studies. Following these studies should come measurement of the emitter deposited/impregnated on suitable substrates, which are chosen so as not to substantially diminish CPL, for example by multiple scattering of emitted photons. The complexes must be robust enough to survive the high temperatures encountered in manufacturing processes such

as lamination. Finally, the overall complex–substrate–laminate composite would ideally be inert towards atmospheric influences and washing with seawater, detergents and solvents.

To conclude, there is now widespread interest in the development of CPL-active Ln^{III} complexes. New strategies have been developed to maximise g_{em} and increase CPB_i . Optical measurement technologies can now rapidly verify CPL signals and perform enantioselective imaging of CPL-active complexes. Further, these CPL analysis technologies are becoming more cost-efficient and could feasibly be adapted for end-user applications. These complementary technological and chemical developments make CPL-active Ln^{III} security inks seem genuinely feasible and have enriched the broader field of CPL-active Ln^{III} complexes, which is set to undergo a renaissance.

[H1] References

1. Andres, J., Hersch, R. D., Moser, J. E. & Chauvin, A. S. A new anti-counterfeiting feature relying on invisible luminescent full color images printed with lanthanide-based inks. *Adv. Funct. Mater.* **24**, 5029–5036 (2014).
Demonstrates that lanthanide luminescence can be used to create full-colour images which are otherwise invisible under room light.
2. Lowe, P. Counterfeiting: links to organised crime and terrorist funding. *J. Financ. Crime* **13**, 255–257 (2006).
3. Soon, J. M. & Manning, L. Developing anti-counterfeiting measures: the role of smart packaging. *Food Res. Int.* **123**, 135–143 (2019).
4. Sonnex, E., Almond, M. J., Baum, J. V. & Bond, J. W. Identification of forged Bank of England £20 banknotes using IR spectroscopy. *Spectrochim. Acta - Part A Mol. Biomol. Spectrosc.* **118**, 1158–1163 (2014).
5. Lau, Y. B., Ar, O. B. N., Anein, Y. H. & Oag, A. B. Meta-hologram-based authentication scheme employing a speckle pattern fingerprint. *Opt. Express* **28**, 8924–8936 (2020).
6. Prime, E. L. & Solomon, D. H. Australia’s plastic banknotes: fighting counterfeit currency. *Angew. Chemie - Int. Ed.* **49**, 3726–3736 (2010).
7. Lancaster, I. M. & Mitchell, A. The growth of optically variable features on banknotes. *Proc. Vol. 5310, Opt. Secur. Counterfeit Deterrence Tech. V* (2004). doi:10.1017/CBO9781107415324.004
8. Baek, S., Choi, E., Baek, Y. & Lee, C. Detection of counterfeit banknotes using multispectral images. *Digit. Signal Process. A Rev. J.* **78**, 294–304 (2018).
9. Zheng, Y. *et al.* Unclonable plasmonic security labels achieved by shadow-mask-lithography-assisted self-assembly. *Adv. Mater.* **28**, 2330–2336 (2016).
10. Yeh, C.-H., Sung, P.-Y., Kuo, C.-H. & Yeh, R.-N. Robust laser speckle recognition system for authenticity identification. *Opt. Express* **20**, 24382–24393 (2012).
11. Carro-Temboury, M. R., Arppe, R., Vosch, T. & Sørensen, T. J. An optical authentication system based on imaging of excitation-selected lanthanide luminescence. *Sci. Adv.* **4**, e1701384 (2018).
12. Arppe, R. & Sørensen, T. J. Physical unclonable functions generated through chemical

methods for anti-counterfeiting. *Nat. Rev. Chem.* **1**, 0031 (2017).

Excellent introduction to anti-counterfeiting technologies.

13. Martins, A. R., Talhavini, M., Vieira, M. L., Zacca, J. J. & Braga, J. W. B. Discrimination of whisky brands and counterfeit identification by UV–Vis spectroscopy and multivariate data analysis. *Food Chem.* **229**, 142–151 (2017).
14. de Almeida, M. R., Correa, D. N., Rocha, W. F. C., Scafi, F. J. O. & Poppi, R. J. Discrimination between authentic and counterfeit banknotes using raman spectroscopy and PLS-DA with uncertainty estimation. *Microchem. J.* **109**, 170–177 (2013).
15. Guedes, A. *et al.* Raman microspectroscopy of genuine and fake euro banknotes. *Spectrosc. Lett.* **46**, 569–576 (2013).
16. Imperio, E., Calò, E., Valli, L. & Giancane, G. Spectral investigations on 1000 £ banknotes throughout Italian Republic. *Vib. Spectrosc.* **79**, 52–58 (2015).
17. Novais Rodrigues, A. R., Melquiades, F. L., Appoloni, C. R. & Marques, E. N. Characterization of Brazilian banknotes using portable X-ray fluorescence and Raman spectroscopy. *Forensic Sci. Int.* **302**, 109872 (2019).
18. Li, H. *et al.* The design of room-temperature-phosphorescent carbon dots and their application as a security ink. *J. Mater. Chem. C* **7**, 10605–10612 (2019).
19. Kalytchuk, S., Wang, Y., Poláková, K. & Zbořil, R. Carbon dot fluorescence-lifetime-encoded anti-counterfeiting. *ACS Appl. Mater. Interfaces* **10**, 29902–29908 (2018).
20. Hartl, A., Grubert, J., Schmalstieg, D. & Reitmayr, G. Mobile interactive hologram verification. *2013 IEEE Int. Symp. Mix. Augment. Reality, ISMAR 2013* 75–82 (2013). doi:10.1109/ISMAR.2013.6671766
21. Kumar, P., Dwivedi, J. & Gupta, B. K. Highly luminescent dual mode rare-earth nanorod assisted multi-stage excitable security ink for anti-counterfeiting applications. *J. Mater. Chem. C* **2**, 10468–10475 (2014).
22. Singh, A. K., Singh, S. & Gupta, B. K. Highly efficient, chemically stable, and UV/blue-light-excitable biluminescent security ink to combat counterfeiting. *ACS Appl. Mater. Interfaces* **10**, 44570–44575 (2018).
23. Štolc, S., Wild, P., Valentin, K., Daubner, F. & Clabian, M. On interoperability of security document reading devices. *Proc. - 2016 Eur. Intell. Secur. Informatics Conf. EISIC 2016* 9–15 (2017). doi:10.1109/EISIC.2016.011
24. Valentín, K., Wild, P., Štolc, S., Daubner, F. & Clabian, M. Optical benchmarking of security document readers for automated border control. *Opt. Photonics Counterterrorism, Crime Fight. Def. XII* 999503 (2016).
25. Tian, Z. *et al.* Conjugated polymer nanoparticles incorporating antifade additives for improved brightness and photostability. *J. Phys. Chem. B* **117**, 4517–4520 (2013).
26. Belair, S. D., Maupin, C. L., Logue, M. W. & Riehl, J. P. Analysis of the temperature dependence of the racemization of Eu(III) complexes through measurement of steady-state circularly polarized luminescence. *J. Lumin.* **86**, 61–66 (2000).

An important paper validating the pivotal aspect of anti-counterfeit application of enantioselective lanthanide complexes with respect to resistance towards heigh

temperature induced racemisation.

27. Frawley, A. T., Pal, R. & Parker, D. Very bright, enantiopure europium(III) complexes allow time-gated chiral contrast imaging. *Chem. Commun.* **52**, 13349–13352 (2016).

Demonstrates enantioselective CPL epifluorescence microscopy of a europium(III) complex impregnated into a paper substrate.

28. Mahesh, S., Lekshmi, C. L., Renuka, K. D. & Joseph, K. Simple and cost-effective synthesis of fluorescent graphene quantum dots from honey: application as stable security ink and white-light emission. *Part. Part. Syst. Charact.* **33**, 70–74 (2016).
29. Zinna, F. & Di Bari, L. Emerging field of chiral Ln(III) complexes for OLEDs. in *Lanthanide-Based Multifunctional Materials* (eds. Martin-Ramos, P. & Ramos-Silva, M.) 171–194 (Elsevier, 2018). doi:10.1016/b978-0-12-813840-3.00005-3
30. Piguet, C. Set aside when building the periodic table 150 years ago, are rare earths any better considered by chemists in the 21 st century? *Chimia (Aarau)*. **73**, 165–172 (2019).
31. Binnemans, K. Interpretation of europium(III) spectra. *Coord. Chem. Rev.* **295**, 1–45 (2015).
32. Friedman, H. G., Choppin, G. R. & Feuerbacher, D. G. The shapes of the f orbitals. *J. Chem. Educ.* **41**, 354–358 (1964).

An excellent introduction to the f orbitals, an understanding of which is essential to discussing the photophysical properties of lanthanide complexes.

33. Bünzli, J. C. G. Rising stars in science and technology: luminescent lanthanide materials. *Eur. J. Inorg. Chem.* **2017**, 5058–5063 (2017).
34. Van Vleck, J. H. The puzzle of rare-earth spectra in solids. *J. Phys. Chem.* **41**, 67–80 (1937).
35. Bünzli, J. C. G. & Eliseeva, S. V. Intriguing aspects of lanthanide luminescence. *Chem. Sci.* **4**, 1939–1949 (2013).
36. Butler, S. J. *et al.* EuroTracker dyes: highly emissive europium complexes as alternative organelle stains for live cell imaging. *Chem. Sci.* **5**, 1750–1756 (2014).
37. Muller, G. Luminescent chiral lanthanide(III) complexes as potential molecular probes. *Dalt. Trans.* **44**, 9692–9707 (2009).
38. Krasnoperov, L. N., Marras, S. A. E., Kozlov, M., Wirpsza, L. & Mustaev, A. Luminescent probes for ultrasensitive detection of nucleic acids. *Bioconjug. Chem.* **21**, 319–327 (2010).
39. Petoud, S. *et al.* Brilliant Sm, Eu, Tb, and Dy chiral lanthanide complexes with strong circularly polarized luminescence. *J. Am. Chem. Soc.* **129**, 77–83 (2007).

Provides examples of characteristic luminescence from Tb, Eu, Dy, and Sm complexes and demonstrates application of two chiral enantiomeric octadentate ligand systems to producing CPL via complexation with Tb, Eu, Dy, and Sm ions.

40. Ayers, K. M., Schley, N. D. & Ung, G. Circularly polarized luminescence from enantiopure C₂-symmetrical tetrakis(2-pyridylmethyl)-1,2-diaminocyclohexane lanthanide complexes. *Inorg. Chem.* **59**, 7657–7665 (2020).
 41. Maupin, C. L., Parker, D., Williams, J. A. G. C. polarized luminescence from chiral octadentate complexes of Y. in the near-infrared & Riehl, J. P. Circularly polarized luminescence from chiral octadentate complexes of Yb(III) in the near-infrared. *J. Am. Chem. Soc.* **120**, 10563–10564 (1998).
 42. Maupin, C. L. *et al.* The measurement of circular polarization in the near-IR luminescence from chiral complexes of Yb(III) and Nd(III). *J. Phys. Chem. A* **104**, 6709–6717 (2000).
 43. Doistau, B., Jiménez, J.-R. & Piguet, C. Beyond chiral organic (p-block) chromophores for circularly polarized luminescence: the success of d-block and f-block chiral complexes. *Front. Chem.* **8**, (2020).
 44. Peijzel, P. S., Meijerink, A., Wegh, R. T., Reid, M. F. & Burdick, G. W. A complete 4fn energy level diagram for all trivalent lanthanide ions. *J. Solid State Chem.* **178**, 448–453 (2005).
 45. Kakkar, T., Thomas, N., Kumi-Barimah, E., Jose, G. & Saha, S. Photoluminescence intensity ratio of Eu-conjugated lactates — a simple optical imaging technique for biomarker analysis for critical diseases. *J. Biophotonics* **11**, e201700199 (2018).
 46. Starck, M., Pal, R. & Parker, D. Structural control of cell permeability with highly emissive europium(III) complexes permits different microscopy applications. *Chem. - A Eur. J.* **22**, 570–580 (2016).
 47. Dai, L. *et al.* Synthesis of water-soluble chiral DOTA lanthanide complexes with predominantly twisted square antiprism isomers and circularly polarized luminescence. *Inorg. Chem.* **58**, 12506–12510 (2019).
 48. Mackenzie, L. E. *et al.* The theoretical molecular weight of NaYF₄:RE upconversion nanoparticles. *Sci. Rep.* **8**, 1106 (2018).
 49. Nampi, P. P. *et al.* Selective cellular imaging with lanthanide based upconversion nanoparticles. *J. Biophotonics* **12**, e201800256 (2018).
 50. Sugimoto, M. *et al.* Circularly polarized luminescence from inorganic materials: encapsulating guest lanthanide oxides in chiral silica hosts. *Chem. - a Eur. J.* **24**, 6519–6524 (2018).
 51. Kumar, J., Marydasan, B., Nakashima, T., Kawai, T. & Yuasa, J. Chiral supramolecular polymerization leading to eye differentiable circular polarization in luminescence. *Chem. Commun.* **52**, 9885–9888 (2016).
- Demonstrated new strategy to boost CPL emission {Eu[(+)-hfbc]4} from +1.38 (monomeric form) to glum = +1.45 via polymerisation into a helical aggregate.**
52. Cerdán, L. *et al.* Circularly polarized laser emission in optically active organic dye solutions. *Phys. Chem. Chem. Phys.* **19**, 22088–22093 (2017).
 53. Jiménez, J. *et al.* Chiral organic dyes endowed with circularly polarized laser emission. *J. Phys. Chem. C* **121**, 5287–5292 (2017).

54. Wu, Y. *et al.* Rational design of circularly polarized luminescent AIEgens: promoting dissymmetry factor and emission efficiency synchronously. *ACS Mater.* **2**, 505–510 (2020).
55. Wan, L. *et al.* Inverting the handedness of circularly polarized luminescence from light-emitting polymers using film thickness. *ACS Nano* **13**, 8099–8105 (2019).
56. Raman, C. V. & Bhagavantam, S. Experimental proof of the spin of the photon. *Nature* **129**, 22–23 (1932).
57. Beth, R. A. Mechanical detection and measurement of the angular momentum of light. *Phys. Rev.* **50**, 115–125 (1936).
58. Foss, J. G. Photonic angular momentum and selection rules for rotational transitions. *J. Chem. Educ.* **47**, 778–779 (1970).
59. Andrews, D. L. Chirality in fluorescence and energy transfer. *Methods Appl. Fluoresc.* **7**, (2019).
60. Torigoe, E. Representing circular polarization with a box of cereal. *Phys. Teach.* **50**, 188–188 (2012).
61. Shah, A. & Ghalsasi, P. Use of interference colours to distinguish between fast and slow axes of a quarter wave plate. *Eur. J. Phys.* **40**, (2019).
62. Schmitzer, H., Tierney, D. & Toepker, T. Real 3-D: how does it work? *Phys. Teach.* **47**, 456–459 (2009).
63. Chiou, T.-H. *et al.* Circular polarization vision in a stomatopod crustacean. *Curr. Biol.* **18**, 429–434 (2008).
64. Roberts, N. W., Chiou, T. H., Marshall, N. J. & Cronin, T. W. A biological quarter-wave retarder with excellent achromaticity in the visible wavelength region. *Nat. Photonics* **3**, 641–644 (2009).
65. Brady, P. & Cummings, M. Differential response to circularly polarized light by the jewel scarab beetle *Chrysina gloriosa*. *Am. Nat.* **175**, 614–620 (2010).
66. Warrant, E. J. Polarisation vision: beetles see circularly polarised light. *Curr. Biol.* **20**, R610–R612 (2010).
67. Shurcliff, W. A. Haidinger's brushes and circularly polarized light. *J. Opt. Soc. Am.* **45**, 399 (1955).
68. Temple, S. E. *et al.* Perceiving polarization with the naked eye: characterization of human polarization sensitivity. *Proc. R. Soc. B Biol. Sci.* **282**, 20150338 (2015).
69. Kew, W., Goodall, I., Clarke, D. & Uhrín, D. Chemical diversity and complexity of scotch whisky as revealed by high-resolution mass spectrometry. *J. Am. Soc. Mass Spectrom.* **28**, 200–213 (2017).
70. Chen, Y. *et al.* Hollow/rattle-type mesoporous nanostructures by a structural difference-based selective etching strategy. *ACS Nano* **4**, 529–539 (2010).
71. Meier, W. Polymer nanocapsules. *Chem. Soc. Rev.* **29**, 295–303 (2000).
72. Mackenzie, L. E., Pålsson, L.-O., Parker, D., Beeby, A. & Pal, R. Rapid time-resolved circular polarization luminescence (CPL) emission spectroscopy. *Nat. Commun.* **11**,

1676 (2020).

Reports the first next-generation rapid SS-CPL spectrometer and demonstrates time-gated CPL measurement in as little as 10 ms.

73. Bruce, J. I., Parker, D., Lopinski, S. & Peacock, R. D. Survey of factors determining the circularly polarised luminescence of macrocyclic lanthanide complexes in solution. *Chirality* **14**, 562–567 (2002).
74. Arrico, A. L., Di Bari, L. & Zinna, F. Quantifying the overall efficiency of circularly polarized emitters. *Chem. - A Eur. J.* (2020). doi:10.1002/chem.202002791

Reports CPB values for over 180 compounds.

75. Zhou, Y., Li, H., Zhu, T., Gao, T. & Yan, P. A highly luminescent chiral tetrahedral Eu₄L₄(L')₄ cage: chirality induction, chirality memory, and circularly polarized luminescence. *J. Am. Chem. Soc.* **141**, 19634–19643 (2019).
76. Lunkley, J. L., Shirotani, D., Yamanari, K., Kaizaki, S. & Muller, G. Extraordinary circularly polarized luminescence activity exhibited by cesium tetrakis (3-heptafluorobutylryl-(+)- camphorato) Eu(III) complexes in EtOH and CHCl₃ solutions. *J. Am. Chem. Soc.* **130**, 13814–13815 (2008).
77. Lunkley, J. L., Shirotani, D., Yamanari, K., Kaizaki, S. & Muller, G. Chiroptical spectra of a series of tetrakis((+)-3- heptafluorobutylrylcamphorato)lanthanide(III) with an encapsulated alkali metal ion: circularly polarized luminescence and absolute chiral structures for the Eu(III) and Sm(III) complexes. *Inorg. Chem.* **50**, 12724–12732 (2011).

Reported Cs{Eu[(+)-hfbc]₄} complex with extraordinarily high CPL, glum = +1.38.

78. Kitagawa, Y. *et al.* Chiral lanthanide lumino-glass for a circularly polarized light security device. *Commun. Chem.* **3**, 1–5 (2020).

Demonstrates enantioselective CPL imaging with a high glum (±1.2) europium(III) complex on a glass substrate.

79. Frawley, A. T., Pal, R. & Parker, D. Very bright, enantiopure europium(III) complexes allow time-gated chiral contrast imaging. *Chem. Commun.* **52**, 13349–13352 (2016).
80. Sánchez-Carnerero, E. M. *et al.* Circularly polarized luminescence from simple organic molecules. *Chem. - A Eur. J.* **21**, 13488–13500 (2015).

A substantial review article providing excellent context for CPL spectroscopy in general and details the operation and calibration of legacy SM-CPL spectrometers.

81. Metcalf, D. H. *et al.* Excited-state chiral discrimination observed by time-resolved circularly polarized luminescence measurements. *J. Am. Chem. Soc.* **111**, 3082–3083 (1989).
82. Metcalf, D. H., Demas, J. N., Richardson, F. S. & Snyder, S. W. Chiral discrimination in electronic energy-transfer processes between dissymmetric metal complexes in solution. Time-resolved chiroptical luminescence measurements of enantioselective excited-state quenching kinetics. *J. Am. Chem. Soc.* **112**, 5681–5695 (1990).

83. Schauerte, J. A., Steel, D. G. & Gafni, A. Time-resolved circularly polarized protein phosphorescence. *Proc. Natl. Acad. Sci.* **89**, 10154–10158 (1992).
84. Schauerte, J. A., Schlyer, B. D., Steel, D. G. & Gafni, A. Nanosecond time-resolved circular polarization of fluorescence: study of NADH bound to horse liver alcohol dehydrogenase. *Proc. Natl. Acad. Sci.* **92**, 569–573 (1995).
85. Meskers, S. C. J. & Dekkers, H. P. J. M. Enantioselective quenching of luminescence: molecular recognition of chiral lanthanide complexes by biomolecules in solution. *J. Phys. Chem. A* **105**, 4589–4599 (2001).
86. Blok, P., Schakel, P. & Dekkers, H. Time-resolved and continuous-wave circular polarisation of luminescence spectroscopy using a commercial spectrofluorimeter. *Meas. Sci. Technol.* **126**, 126–130 (1990).
87. Glover-Fischer, D. P. *et al.* Excited-state enantiomer interconversion kinetics probed by time-resolved chiroptical luminescence spectroscopy. The solvent and temperature dependence of Δ -enantiomer interconversion rates in solution. *Inorg. Chem.* **37**, 3026–3033 (1998).
88. Beeby, A., Pal, R. & Palsson, L.-O. Light detecting apparatus for simultaneously detecting left- and right-handed circularly polarised light. Worldwide patent WO2016174395A1. (2016).
89. Gendron, F. *et al.* Luminescence, chiroptical, magnetic and ab-initio crystal-field characterizations of an enantiopure helicoidal Yb (III) complex : the van Vleck renaissance.
90. Frawley, A. T., Linford, H. V., Starck, M., Pal, R. & Parker, D. Enantioselective cellular localisation of europium(III) coordination complexes. *Chem. Sci.* **9**, 1042–1049 (2018).
91. Tsumatori, H., Nakashima, T. & Kawai, T. Observation of chiral aggregate growth of perylene derivative in opaque solution by circularly polarized luminescence. *Org. Lett.* **12**, 2362–2365 (2010).
92. Imai, Y., Nakano, Y., Kawai, T. & Yuasa, J. A smart sensing method for object identification using circularly polarized luminescence from coordination-driven self-assembly. *Angew. Chemie - Int. Ed.* **57**, 8973–8978 (2018).
93. Tsumatori, H., Harada, T., Yuasa, J., Hasegawa, Y. & Kawai, T. Circularly polarized light from chiral lanthanide(III) complexes in single crystals. *Appl. Phys. Express* **4**, 17–20 (2011).
94. Kumar, J. *et al.* Circularly polarized luminescence in supramolecular assemblies of chiral bichromophoric perylene bisimides. *Chem. - A Eur. J.* **19**, 14090–14097 (2013).
95. Katayama, K., Hirata, S. & Vacha, M. Circularly polarized luminescence from individual microstructures of conjugated polymer aggregates with solvent-induced chirality. *Phys. Chem. Chem. Phys.* **16**, 17983–17987 (2014).
96. Koike, H., Nozaki, K. & Iwamura, M. Microscopic imaging of chiral amino acids in agar gel through circularly polarized luminescence of Eu^{III} complex. *Chem. Asian J.* **15**, 85–90 (2020).
97. Mason, S. F., Peacock, R. D. & Stewart, B. Ligand-polarization contributions to the

- intensity of hypersensitive trivalent lanthanide transitions. *Mol. Phys.* **30**, 1829–1841 (1975).
98. Mason, S. F. The ligand polarization model for transition probabilities in the electronic spectra of metal complexes. *J. Mol. Struct.* **60**, 363–366 (1980).
99. Reid, M. F. & Richardson, F. S. Electric dipole intensity parameters for lanthanide 4f→4f transitions. *J. Chem. Phys.* **79**, 5735–5742 (1983).
100. Bonsall, S. D., Houcheime, M., Straus, D. A. & Muller, G. Optical isomers of N,N'-bis(1-phenylethyl)-2,6-pyridinedicarboxamide coordinated to europium(III) ions as reliable circularly polarized luminescence calibration standards. *Chem. Commun.* **35**, 3676–3678 (2007).
101. Hua, K. T. *et al.* Structural and photophysical properties of visible- and near-IR-emitting tris lanthanide(III) complexes formed with the enantiomers of N, N'-bis(1-phenylethyl)-2,6-pyridinedicarboxamide. *Inorg. Chem.* **51**, 647–660 (2012).
102. Starck, M., Mackenzie, L., Batsanov, A. S., Parker, D. & Pal, R. Excitation modulation of Eu:BPEPC based complexes as low-energy reference standards for circularly polarised luminescence (CPL). *Chem. Commun.* **55**, 14115–14118 (2019).
- A suggested new CPL calibration standard to be used with 365 nm UV LED based excitation.**
103. Zinna, F., Giovanella, U. & Di Bari, L. Highly circularly polarized electroluminescence from a chiral europium complex. *Adv. Mater.* **27**, 1791–1795 (2015).
104. Górecki, M., Carpita, L., Arrico, L., Zinna, F. & Di Bari, L. Chiroptical methods in a wide wavelength range for obtaining Ln³⁺ complexes with circularly polarized luminescence of practical interest. *Dalt. Trans.* **47**, 7166–7177 (2018).
105. Butler, S. J. *et al.* Utility of tris(4-bromopyridyl) europium complexes as versatile intermediates in the divergent synthesis of emissive chiral probes. *Dalt. Trans.* **43**, 5721–5730 (2014).
106. Zhou, Y. *et al.* Point chirality controlled diastereoselective self-assembly and circularly polarized luminescence in quadruple-stranded europium(III) helicates. *Inorg. Chem.* **59**, 12850–12857 (2020).
- Reports tetrahedral Eu(III) complexes with extraordinarily high CPB values of >1000 and >3000 M⁻¹cm⁻¹.**
107. Brittain, H. G. & Richardson, F. S. Circularly polarized emission studies on the chiral nuclear magnetic resonance lanthanide shift reagent tris(3-trifluoroacetyl-d-camphorato)europium(III). *J. Am. Chem. Soc.* **98**, 5858–5863 (1976).
- An excellent example of the legacy SM-PEM-CPL spectrometer, establishing the use of Eu(facam)₃ as a CPL reference standard**
108. Zinna, F. *et al.* Circularly polarized luminescence under near-UV excitation and structural elucidation of a Eu complex. *Chem. Commun.* **51**, 11903–11906 (2015).
109. Harada, T. *et al.* Circularly polarized luminescence from chiral Eu(III) complex with high emission quantum yield. *J. Alloys Compd.* **488**, 599–602 (2009).

110. Harada, T. *et al.* Nona-coordinated chiral Eu(III) complexes with stereoselective ligand-ligand noncovalent interactions for enhanced circularly polarized luminescence. *Inorg. Chem.* **51**, 6476–6485 (2012).
111. Bozoklu, G. *et al.* Metal-controlled diastereoselective self-assembly and circularly polarized luminescence of a chiral heptanuclear europium wheel. *J. Am. Chem. Soc.* **134**, 8372–8375 (2012).
112. Arrico, L., Rosa, C. De, Di Bari, L., Melchior, A. & Piccinelli, F. Effect of the counterion on circularly polarized luminescence of europium(III) and samarium(III) complexes. *Inorg. Chem.* **59**, 5050–5062 (2020).
113. Seitz, M., Moore, E. G., Ingram, A. J., Muller, G. & Raymond, K. N. Enantiopure, octadentate ligands as sensitizers for europium and terbium circularly polarized luminescence in aqueous solution. *J. Am. Chem. Soc.* **129**, 15468–15470 (2007).
114. Wada, S. *et al.* The relationship between magneto-optical properties and molecular chirality. *NPG Asia Mater.* **8**, e251 (2016).
115. Lama, M. *et al.* Lanthanide class of a trinuclear enantiopure helical architecture containing chiral ligands: synthesis, structure, and properties. *Chem. - A Eur. J.* **13**, 7358–7373 (2007).
116. Leonzio, M. *et al.* Strongly circularly polarized emission from water-soluble Eu(III)- and Tb(III)-based complexes: a structural and spectroscopic study. *Inorg. Chem.* **56**, 4413–4422 (2017).
117. Seitz, M. *et al.* Circularly polarized luminescence in enantiopure europium and terbium complexes with modular, all-oxygen donor ligands. *Inorg. Chem.* **48**, 8469–8479 (2009).
118. Dickins, R. S. *et al.* Synthesis, time-resolved luminescence, NMR spectroscopy, circular dichroism and circularly polarised luminescence studies of enantiopure macrocyclic lanthanide tetraamide complexes. *Chem. - A Eur. J.* **5**, 1095–1105 (1999).
119. Schnable, D. *et al.* Synthesis of enantiopure lanthanide complexes supported by hexadentate N, N' -bis (methylbipyridyl) bipyrrrolidine and their circularly polarized luminescence. *Inorg. Chem.* **59**, 8498–8504 (2020).
120. Samuel, A. P. S., Lunkley, J. L., Muller, G. & Raymond, K. N. Strong circularly polarized luminescence from highly emissive terbium complexes in aqueous solution. *Eur. J. Inorg. Chem.* **21**, 3343–3347 (2010).
121. Leonard, J. P. *et al.* Self-assembly of chiral luminescent lanthanide coordination bundles. *J. Am. Chem. Soc.* **129**, 10986–10987 (2007).
122. Cotter, D., Dodder, S., Klimkowski, V. J. & Hopkins, T. A. Circularly polarized luminescence of Sm (III) and Eu (III) complexes with chiral ligand (R/S)-BINAPO. *Chirality* **31**, 301–311 (2019).
123. Zinna, F., Arrico, L. & Di Bari, L. Near-infrared circularly polarized luminescence from chiral Yb(III)-diketonates. *Chem. Commun.* **55**, 6607–6609 (2019).
124. Beeby, A. *et al.* Porphyrin sensitization of circularly polarised near-IR lanthanide luminescence: enhanced emission with nucleic acid binding. *Chem. Commun.* **1**, 1183–1184 (2000).

125. Dee, C. *et al.* Strong circularly polarized luminescence of an octahedral chromium(III) complex. *Chem. Commun.* **55**, 13078–13081 (2019).
126. Jiménez, J.-R. *et al.* Chiral molecular ruby [Cr(dqp)₂]³⁺ with long-lived circularly polarized luminescence. *J. Am. Chem. Soc.* **141**, 13244–13252 (2019).
127. Law, G. L. *et al.* Circularly polarized luminescence of curium: a new characterization of the 5f actinide complexes. *J. Am. Chem. Soc.* **134**, 15545–15549 (2012).
128. Liang, J., Guo, P., Qin, X. & Gao, X. Hierarchically chiral lattice self-assembly induced circularly polarized luminescence. *ACS Nano* **14**, 3190–3198 (2020).
129. OuYang, J. & Crassous, J. Chiral multifunctional molecules based on organometallic helicenes: recent advances. *Coord. Chem. Rev.* **376**, 533–547 (2018).
130. Tanaka, H., Inoue, Y. & Mori, T. Circularly polarized luminescence and circular dichroisms in small organic molecules: correlation between excitation and emission dissymmetry factors. *ChemPhotoChem* **2**, 386–402 (2018).
131. Kubo, H., Hirose, T. & Matsuda, K. Control over the emission properties of [5]helicenes based on the symmetry and energy levels of their molecular orbitals. *Org. Lett.* **19**, 1776–1779 (2017).
132. Longhi, G., Castiglioni, E., Abbate, S., Lebon, F. & Lightner, D. A. Experimental and calculated CPL spectra and related spectroscopic data of camphor and other simple chiral cyclic ketones. *Chirality* **25**, 589–599 (2013).
133. Shiraki, T. *et al.* Creation of circularly polarized luminescence from an achiral polyfluorene derivative through complexation with helix-forming polysaccharides: Importance of the meta-linkage chain for helix formation. *Chem. - An Asian J.* **9**, 218–222 (2014).
134. Watanabe, K., Suda, K. & Akagi, K. Hierarchically self-assembled helical aromatic conjugated polymers. *J. Mater. Chem. C* **1**, 2797–2805 (2013).
135. Yang, Y., Da Costa, R. C., Smilgies, D. M., Campbell, A. J. & Fuchter, M. J. Induction of circularly polarized electroluminescence from an achiral light-emitting polymer via a chiral small-molecule dopant. *Adv. Mater.* **25**, 2624–2628 (2013).
136. Zou, C. *et al.* Bacterial cellulose: a versatile chiral host for circularly polarized luminescence. *Molecules* **24**, 1008 (2019).
137. Morisaki, Y., Inoshita, K. & Chujo, Y. Planar-chiral through-space conjugated oligomers: synthesis and characterization of chiroptical properties. *Chem. - A Eur. J.* **20**, 8386–8390 (2014).
138. Jin, X. *et al.* Optically active upconverting nanoparticles with induced circularly polarized luminescence and enantioselectively triggered photopolymerization. *ACS Nano* **13**, 2804–2811 (2019).
139. Clarke, R. *et al.* Circularly polarised luminescence from helically chiral “confused” N,N,O,C -boron-chelated dipyrromethenes (BODIPYs). *ChemPhotoChem* **1**, 513–517 (2017).
140. Sánchez-Carnerero, E. M. *et al.* Circularly polarized luminescence by visible-light absorption in a chiral o-bodipy dye: unprecedented design of cpl organic molecules

- from achiral chromophores. *J. Am. Chem. Soc.* **136**, 3346–3349 (2014).
141. Jiménez, J. *et al.* Modulating ICT emission: a new strategy to manipulate the CPL sign in chiral emitters. *Chem. Commun.* **55**, 1631–1634 (2019).
 142. Li, M. *et al.* Chiral nanoparticles with full-color and white CPL properties based on optically stable helical aromatic imide enantiomers. *ACS Appl. Mater. Interfaces* **10**, 8225–8230 (2018).
 143. Huo, S., Duan, P., Jiao, T., Peng, Q. & Liu, M. Self-assembled luminescent quantum dots to generate full-color and white circularly polarized light. *Angew. Chemie - Int. Ed.* **56**, 12174–12178 (2017).
 144. Tohgha, U. *et al.* Ligand induced circular dichroism and circularly polarized luminescence in cdse quantum dots. *ACS Nano* **7**, 11094–11102 (2013).
 145. Gussakovsky, E. Circularly polarized luminescence (CPL) of proteins and protein complexes. in *Reviews in Fluorescence 2008* 425–459 (2010). doi:10.1007/978-1-4419-1260-2
 146. Cruz, C. M. *et al.* Enantiopure distorted ribbon-shaped nanographene combining two-photon absorption-based upconversion and circularly polarized luminescence. *Chem. Sci.* **9**, 3917–3924 (2018).
 147. Chen, J.-F. *et al.* Planar chiral organoboranes with thermoresponsive emission and circularly polarized luminescence: integration of pillar[5]arenes with boron chemistry. *Angew. Chemie* (2020). doi:10.1002/ange.202001145
 148. Pal *et al.* Simple and versatile modifications allowing time gated spectral acquisition, imaging and lifetime profiling on conventional wide-field microscopes, *Methods Appl. Fluoresc.* **2**, 037001-037007 (2014).

[H1] Acknowledgements

L.E.M. and R.P. acknowledge financial support from the Royal Society URF\R\191002, BBSRC BB/S017615/1, EPSRC EP/P025013/1 and a BBSRC Discovery Fellowship BB/T009268/1.

[H1] Author contributions

L.E.M. conducted review and meta-analysis, wrote the manuscript and designed figures. R.P. Edited the manuscript, designed figures, and conceived the overall direction of the manuscript.

[H1] Competing interest statement

The authors declare no competing interests.

ToC blurb

Several transition metal and lanthanide complexes undergo circularly polarised luminescence. This Review describes design principles for the complexes and instruments used to measure them, including in the context of security inks.

Subject terms

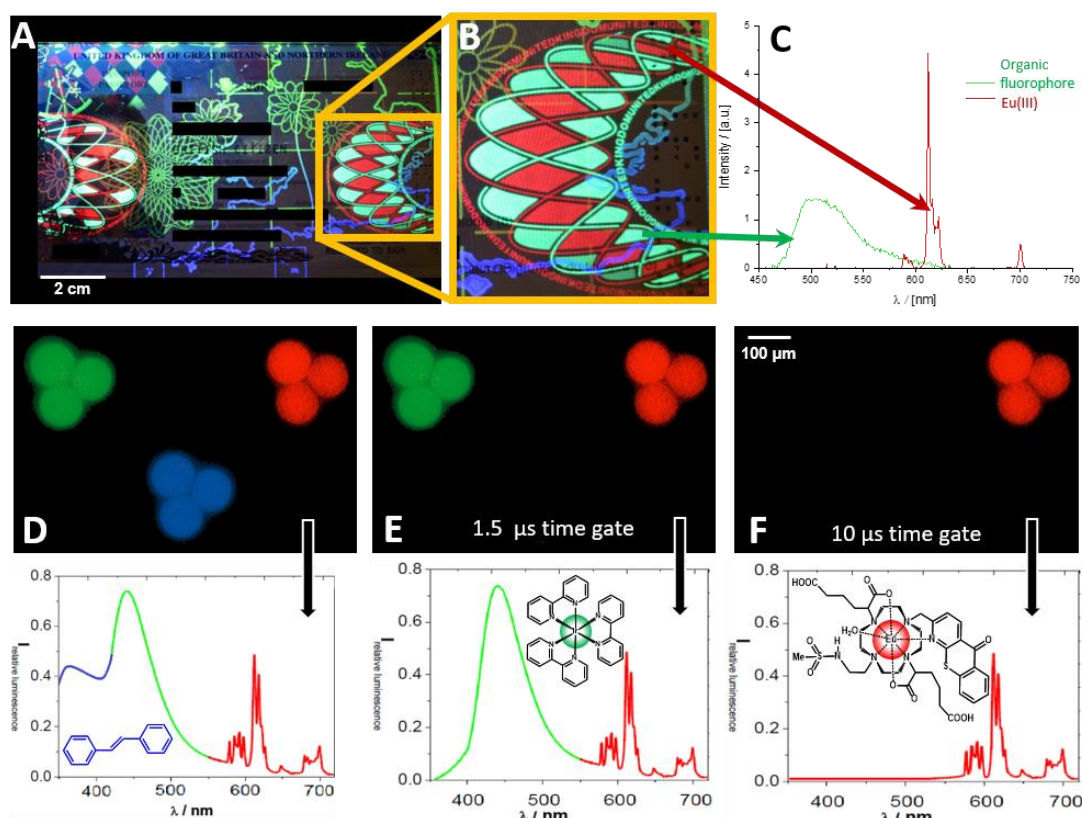


Figure 1 | Security inks featuring long-lived lanthanide luminescence and rapidly emitting organic fluorophores. The multi-component, multi-colour ‘chameleon-like’ inks present different colours under different time-gating regimes. **a** | Luminescent security ink features on a contemporary United Kingdom passport are clearly visible under 365 nm UV-A excitation. **b** | In particular, the patterned section exhibits green and red luminescence. **c** | Emission spectra of the classified security ink components reveals characteristic wide-band green emission from the organic compound and ‘line-like’ red emission from a Eu^{III} complex. **d** | Three ‘chameleon-like’ inks, each with a substantially different emission profile and lifetime, are deposited on a spherical silica substrate. Modified epifluorescence microscope image and simultaneously recorded emission spectra of the red, green and blue fluorophore containing spheres are presented (unpublished data).¹⁴⁸ With no time gating, red emission from a Eu^{III} complex (of a 1,4,7,10-tetraazacyclododecane derivative)¹²⁸, green emission from $[\text{Ir}^{\text{III}}(2,2'\text{-bipyridine})_3]^{3+}$ and blue emission from *trans*-stilbene are all apparent. The emitters can be proportioned to yield overall white emission. **e** | *trans*-Stilbene relaxes quickly, so a 1.5 μs time gate removes its blue emission to give overall orange (red + green) emission. **f** | A 10 μs time gate further removes green emission due to $[\text{Ir}^{\text{III}}(2,2'\text{-bipyridine})_3]^{3+}$, leaving overall red emission. Such verifications would require time-gated illumination and detection apparatus.

Table 1 / Overview of CPL-active molecular systems and features most relevant to security-ink applications. Diverse materials have been tested, with Ln complexes having several advantages over other systems.

CPL-active system	Maximum representative g_{em}	Average CPB_i ($M^{-1}cm^{-1}$) ⁷⁴	Characteristics
Ln complexes	$\sim 0.1-1.4$ (10^0)	Eu ($\Delta J = 1$): 286 Eu ($\Delta J = 2$): 69 Tb: 146 Yb: 4	<ul style="list-style-type: none"> • Strong CPL with distinct fingerprint. • Non-photobleaching. • Emission lifetime ~ 1 ms. • Versatile functionality. Narrow blue, green, red and near infrared emission bands. • g_{em} up to 1.38 ($^5D_0 \rightarrow ^7F_1$) for monomeric complexes.⁷⁶ • g_{em} up to 1.45 ($^5D_0 \rightarrow ^7F_1$) for supramolecular chiral polymers.⁵¹ • Good quantum yields achievable (e.g. $>50\%$).
Cr complexes ^{125,126}	$\sim 10^{-1}$	174	<ul style="list-style-type: none"> • Weak to moderate CPL with enantiomers. • Near-infrared emission. • Emission lifetime ~ 1 ms. • Sensitive to atmospheric gases. • Poor quantum yields ($\sim 1\%$)
Chiral nanotubes from CPL-active chiral subunits ¹²⁸	$\sim 10^{-1}$	N.D.	<ul style="list-style-type: none"> • CPL from chiral subunits amplified by helicity of nanotubes. • Indistinct CPL. • Dopant determines optical properties such as emission wavebands, lifetime and quantum yield.
Helicenes ^{80,129-131}	$\sim 10^{-2}$	5	<ul style="list-style-type: none"> • Fairly weak and indistinct CPL. • Emission colour tuneable. • Low (3%) to good (65%) quantum yields. • Emission lifetime $\sim ns$
Ketones ^{80,132}	$\sim 10^{-2}$	1.1	<ul style="list-style-type: none"> • Weak and indistinct CPL. • Very poor quantum yields ($< 0.1\%$).
Helical polymers ¹³³⁻¹³⁶	$\sim 10^{-2}$	N.D.	<ul style="list-style-type: none"> • Fairly weak and indistinct CPL. • CPL determined by chirality of polymer.
Cyclophanes ^{74,137}	$\sim 10^{-2}$	68	<ul style="list-style-type: none"> • Fairly weak and indistinct CPL.^{74,138} • Good ($>50\%$) quantum yields possible.⁷⁴
Chiral nanotubes with achiral dopants ¹³⁸	$\sim 10^{-3}$	N.D.	<ul style="list-style-type: none"> • Very weak CPL induced by nanotube helicity. • Indistinct CPL. • Dopants determines photophysical properties.
BODIPY derivatives ^{130,139-141}	$\sim 10^{-3}$	47	<ul style="list-style-type: none"> • Very weak and indistinct CPL. • Emission colour tuneable. • Low ($\sim 15\%$) to very good ($\sim 70\%$) quantum yields.

Self-assembled chiral nanoparticles ¹⁴²	$\sim 10^{-3}$	N.D.	<ul style="list-style-type: none"> • Very weak and indistinct CPL. • Emission colour tuneable. • ‘White’ emission possible. • Low quantum yield ($\sim 20\%$).
Quantum dots ^{143,144}	$\sim 10^{-3}$	N.D.	<ul style="list-style-type: none"> • Very weak and indistinct CPL. • Emission colour tuneable.
Proteins ¹⁴⁵	$\sim 10^{-4}$	N.D.	<ul style="list-style-type: none"> • Very weak and indistinct CPL.
Nanographene ¹⁴⁶	$\sim 10^{-4}$	N.D.	<ul style="list-style-type: none"> • Very weak and indistinct CPL. • Emission lifetime ~ 10 ns. • Low quantum yield ($\sim 13\%$).
Organoboranes ¹⁴⁷	$\sim 10^{-5}$	N.D.	<ul style="list-style-type: none"> • Extremely weak and indistinct CPL. • High quantum yields (50–99%). • Emission lifetime ~ 1–10 ns.

CPB_i, circularly polarised brightness for transition *i*; BODIPY, 4,4-difluoro-4-bora-3*a*,4*a*-diazas-indacene; CPL, circularly polarised luminescence; N.D., not determined.

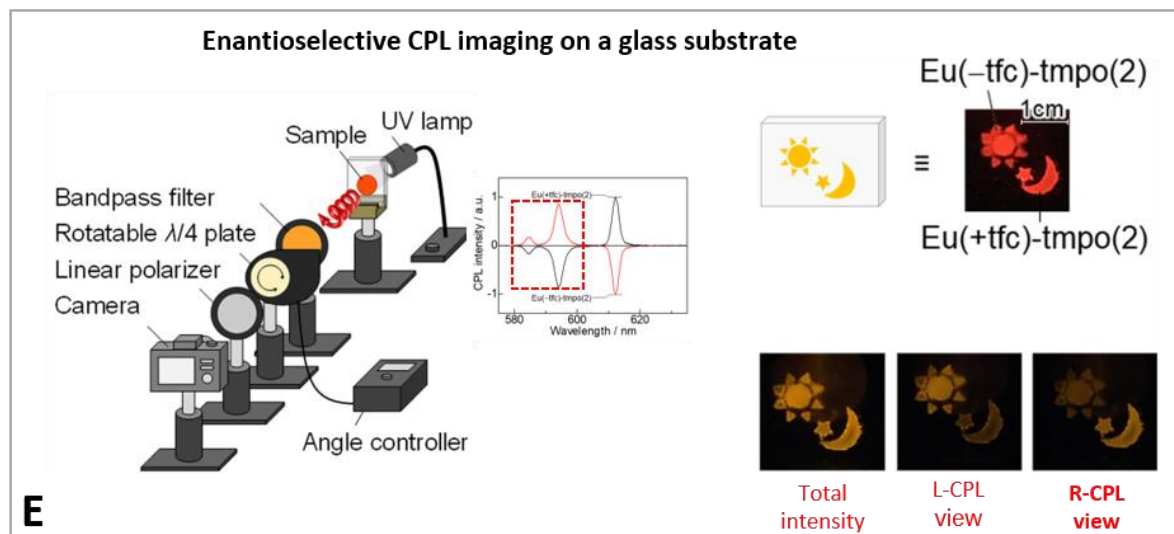
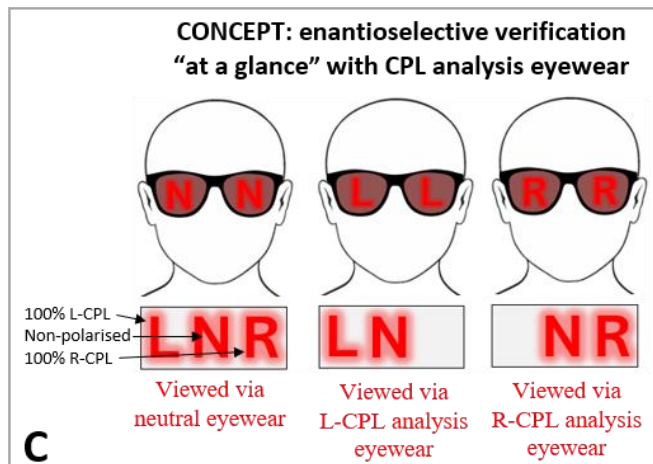
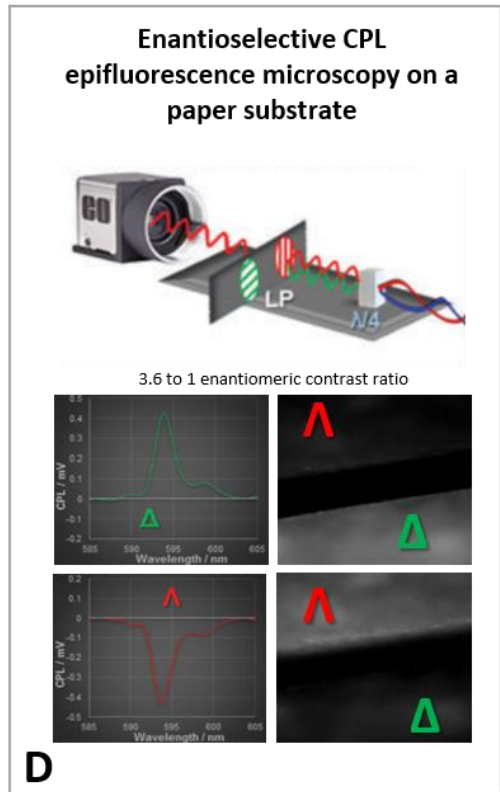
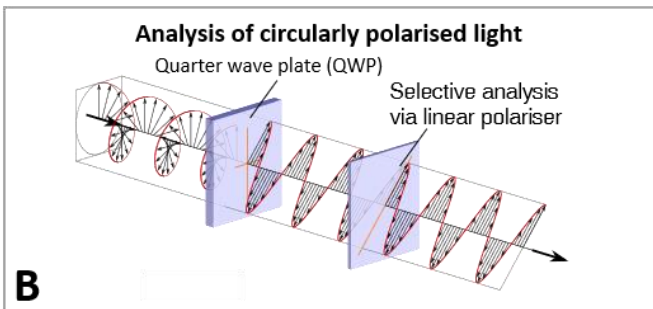
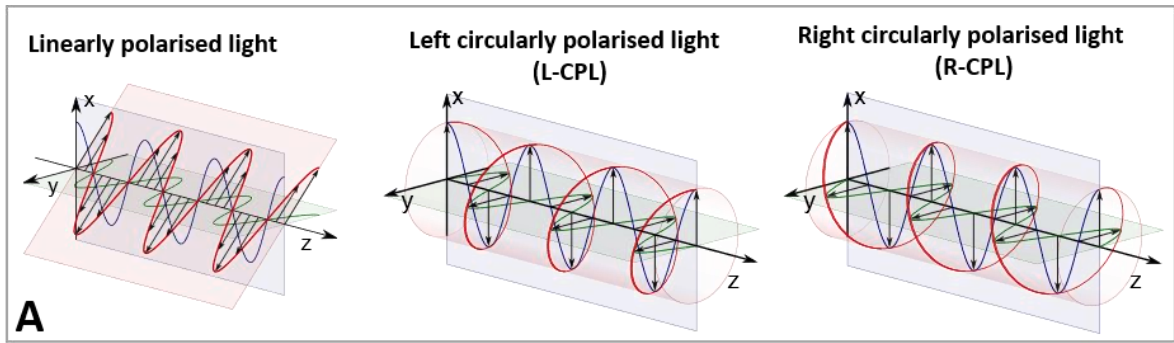


Figure 2 | **Circularly polarised light and enantioselective image contrast.** **a** | Linearly polarised light can be thought of as a superposition of left and right circularly polarised light. The x and y components of the electric field vector are depicted as blue and green lines respectively, with the resultant electric field vector shown as a red line. **b** | L-CPL is converted to linearly polarised light by a quarter wave plate (QWP). R-CPL would produce an orthogonal linearly polarisation state (not shown). A linear polariser can be orientated to allow the linearly polarised light to pass or to be blocked, enabling selective analysis of L-CPL and R-CPL. **c** | Depiction of enantioselective CPL contrast at a glance with eyewear featuring a bandpass filter, QWP and linear polariser. This example depicts exaggerated features — the complete CPL emission ($g_{em} = \pm 2$) here yields perfect enantiomeric contrast. **d** | Enantioselective CPL microscopy of EuL^1 (the N_6O_3 -donor $(\text{L}^1)^{3-}$ is a trivalent tris(pyridylphosphonate) derivative of 1,4,7-triazacyclononane) on a paper substrate gives $g_{em} = \pm \sim|0.10|$ and a 3.6:1 enantiomeric contrast ratio.²⁷ **e** | Selective CPL imaging of two enantiomers of $\{\text{Eu}[(\pm)\text{-3-(trifluoroacetyl)camphor}]_3\}$, deposited with two molar equivalents of tris(2,6-dimethoxyphenyl)phosphine oxide on a glass substrate ($g_{em} = \pm|1.20|$)⁷⁸. Part **d** adapted with permission from Ref. 27, Royal Society of Chemistry. Part **e** adapted with permission from Ref. 78, Springer Nature. g_{em} , emission dissymmetry factor.

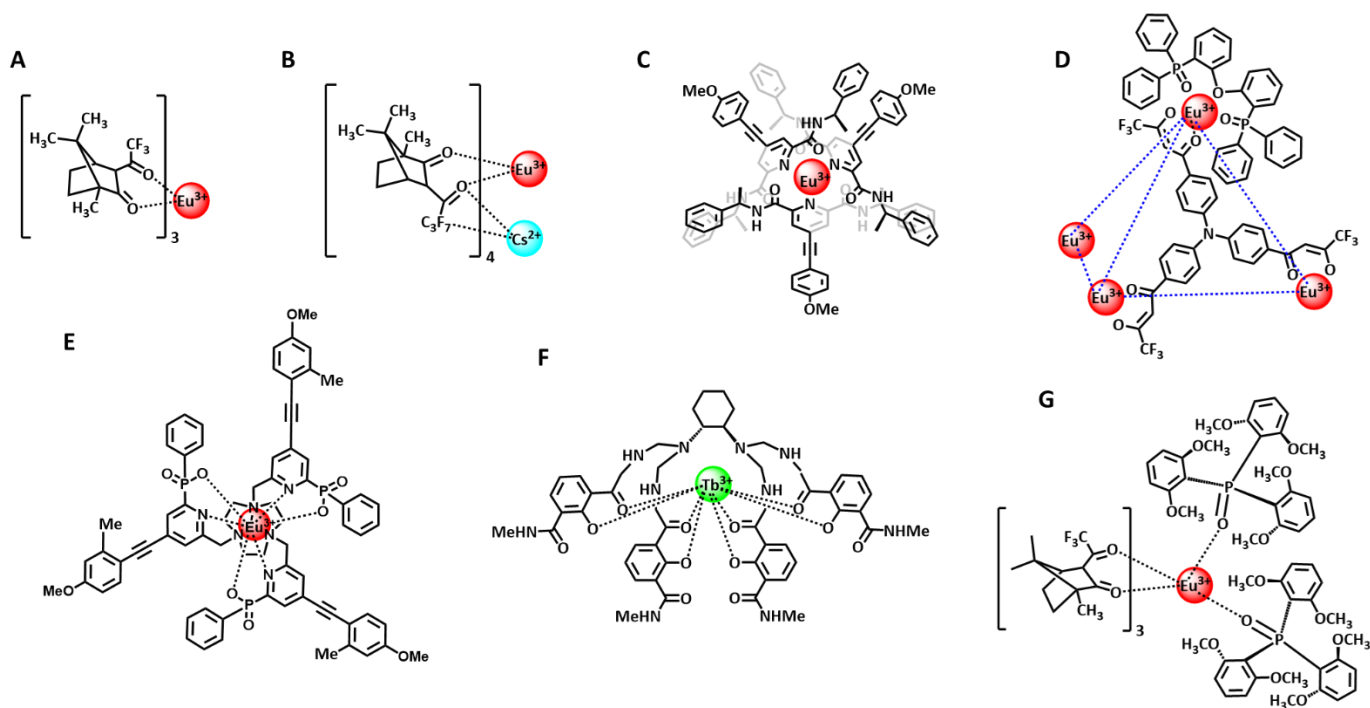


Figure 3 | **A sub-set of chiral lanthanide complexes discussed as candidates for CPL-active security inks.** **a** | $\text{Eu}[(+)\text{-facam}]_3$, a commercially available chiral NMR shift reagent which has found use as a CPL reference standard.^{72,80,107} **b** | $\text{Cs}[\text{Eu}((+)\text{-hfbc})_4]$ exhibits extraordinarily high g_{em} values in monomeric ($\Delta J = 1$, $g_{em} = +1.38$ to $+1.41$) and helical aggregate forms ($\Delta J = 1$, $g_{em} = +1.45$).^{51,76,77} **c** | $\Delta\Delta\Delta\text{-}\{\text{Eu}[(4\text{-methoxyphenyl)alkynyl-bpepc}]_3\}\text{Cl}_3$, recently developed as a UV-A excitable CPL reference standard with good $CPBi$ ($102, 213 \text{ M}^{-1}\text{cm}^{-1}$, $\Delta J = 1, 2$).¹⁰² **d** | $\Delta\Delta\Delta\Delta\text{-}[(\text{Eu}_4\text{L}_4)(\text{DPEPO})_4]$, recently developed as a complex with extraordinarily high $CPBi$ of $1122 \text{ M}^{-1}\text{cm}^{-1}$, **e** | EuL^1 (the N_6O_3 -donor $(\text{L}^1)^{3-}$ is a trivalent tris(pyridylphosphonate) derivative of 1,4,7-triazacyclononane) which has been exploited for enantioselective CPL imaging on a paper substrate.²⁷ **f** | $[\text{Tb}(\text{HL}^2)]$, a UV-A excitable Tb(III)

complex with good $CPBi$ of $194.7 \text{ M}^{-1}\text{cm}^{-1}$. **g** $\{\text{Eu}[(+)\text{-}3\text{-}(\text{trifluoroacetyl})\text{camphorate}]_3\}$ -bis-[tris(2,6-dimethoxyphenyl)phosphine oxide] exhibits high g_{em} values ($g_{em} = -1.2$, $\Delta J = 1$), which has been incorporated into a glass substrate for enantioselective CPL imaging.

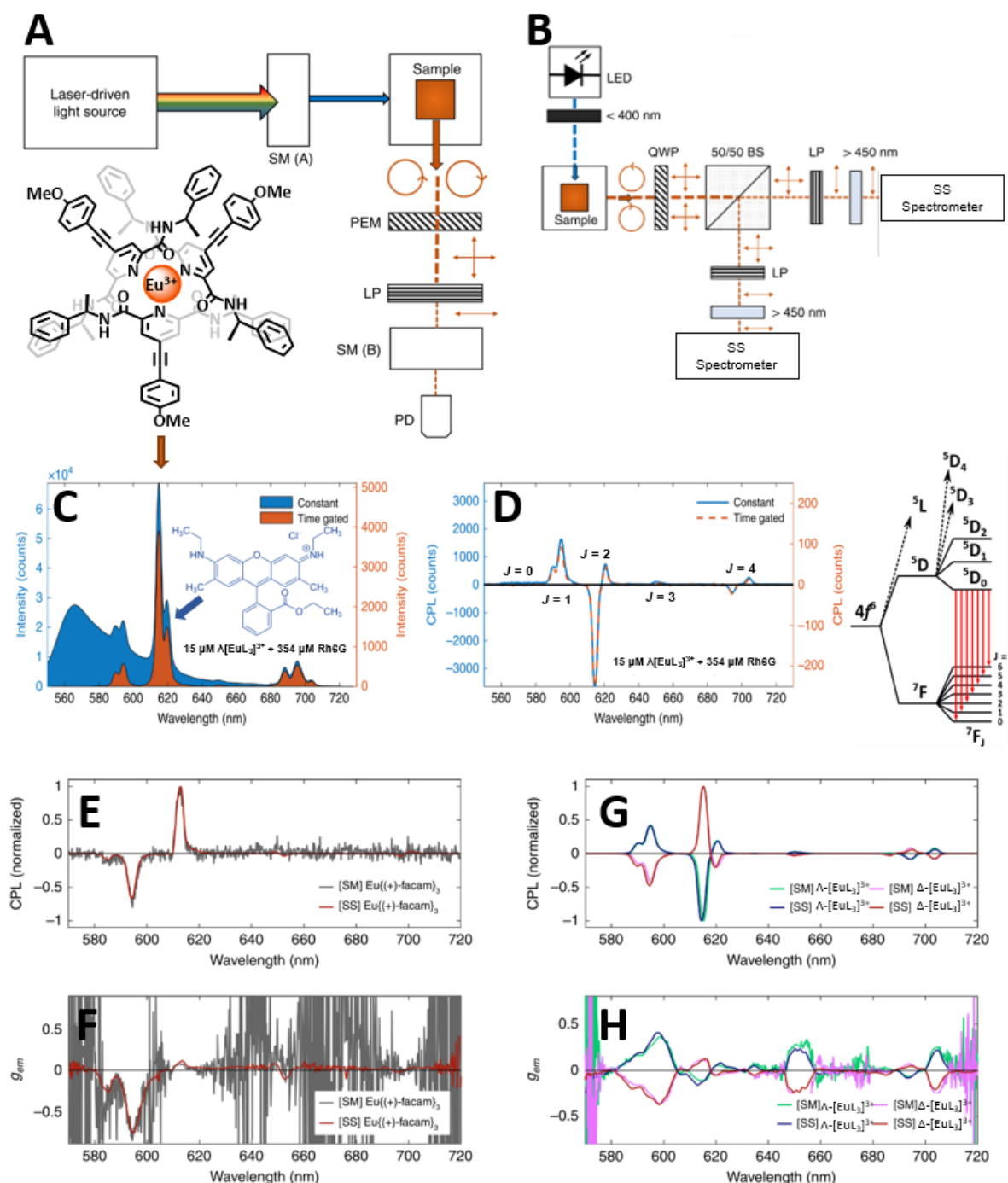


Figure 4 | Next-generation CPL spectrometers have time-gated detection and improved SNR relative to legacy CPL spectrometers. a | Legacy CPL spectrometers are bulky, expensive and slow to acquire data. **b** | A next-generation rapid CPL spectrometer (SS-CPL), can acquire a spectrum in as little as 10 ms. **c** | Time-gated measurement with the SS-CPL spectrometer separates short-lived (\sim ns) luminescence of rhodamine 6G from long-lived (\sim ms) luminescence from $\{\text{Eu}[(4\text{-methoxyphenyl})\text{alkynyl-bpepc}]_3\}\text{Cl}_3$ ($[\text{EuL}_3]^{3+}$ in the original publication). **d** | The CPL spectra of the Eu^{III} complex recovered by normal and time-gated

CPL measurement are identical. The energy levels associated with characteristic Eu^{III} emission bands are shown. **e** | CPL spectrum of the NMR-shift reagent {Eu[(+)-3-(trifluoroacetyl)camphorato]₃} as measured with a legacy CPL spectrometer (grey) next-generation CPL spectrometer (red) demonstrating a dramatic difference in recovered signal-to-noise ratio at 595 nm (18 vs 148) due to rapid accumulation and averaging of spectra. **f** | g_{em} estimates from CPL measurements in **e**. **g,h** | Similar to **e** and **f**, but measurement of CPL emission and g_{em} from enantiomers of {Eu[(4-methoxyphenyl)alkynyl-bpepc]₃}Cl₃. CPL spectra and CPL spectrometer diagrams adapted with permission from Ref.,72, Springer Nature; structure and energy levels for {Eu[(4-methoxyphenyl)alkynyl-bpepc]₃}Cl₃ reproduced with permission from Ref.102, Royal Society of Chemistry. . BS, beam splitter; CPL, circularly polarised luminescence; g_{em} , emission dissymmetry factor; LP, linear polariser; PD, photodiode; PEM, photoelastic modulator; QWP, quarter wave plate; SM, scanning monochromator; SS, solid-state.

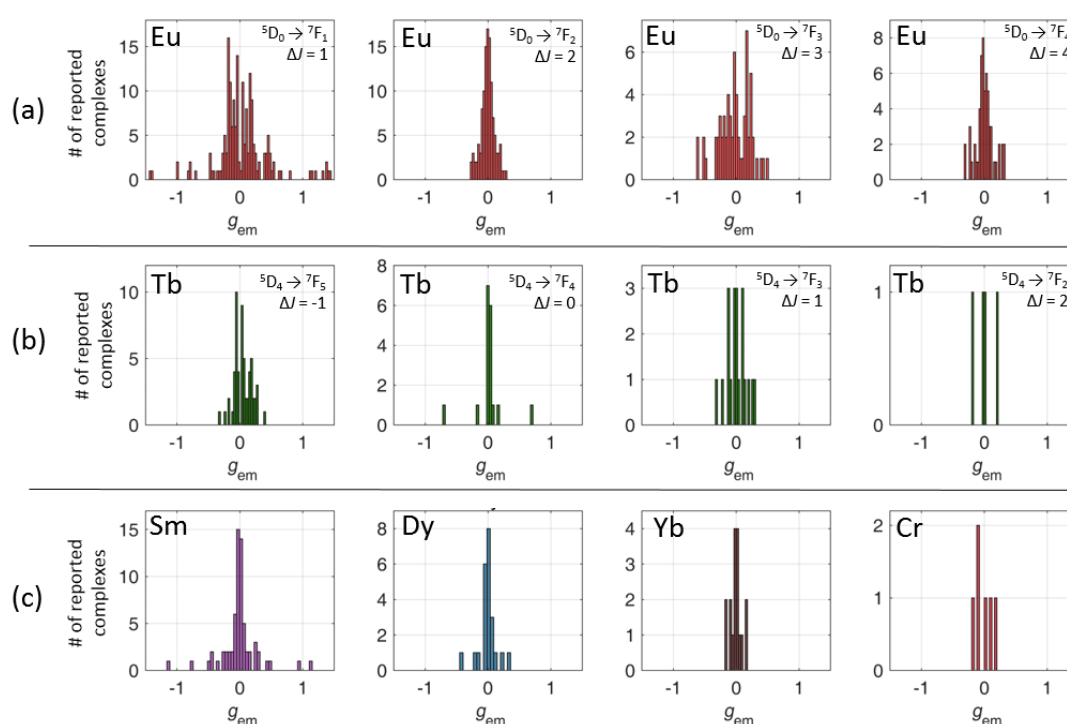


Figure 5 | Reported g_{em} values for CPL-active lanthanide and Cr^{III} complexes discussed here. **a** | Eu^{III} emission bands for $\Delta J = 1, 2, 3, 4$ transitions. The $\Delta J = 1$ emission band (~595 nm) affords the largest g_{em} values, with the $\Delta J = 3$ emission band (~654 nm) giving more modest g_{em} values. The $\Delta J = 2$ and 4 bands give rise to a more constrained range of g_{em} values. **b** | Tb^{III} emission bands have a greater propensity to give lower g_{em} values. **c** | g_{em} values for Sm^{III}, Dy^{III}, Yb^{III} and Cr^{III} complexes are shown for all wavebands because fewer examples of these complexes are reported. Sm^{III} complexes feature a similar range of g_{em} values to those of Eu^{III} complexes but the largest values are $\sim|1.15|$ and arise from only a single complex, Cs[Sm((+)-3-heptafluorobutyryl camphorate)₄], the analogue of the strong CPL emitter Cs[Eu((+)-3-heptafluorobutyryl camphorate)₄] ($g_{em} \sim|1.4|$). For a complex to be included in this dataset, at least one CPL band has to emit with $g_{em} \sim|0.05|$. CPL, circularly polarised luminescence.

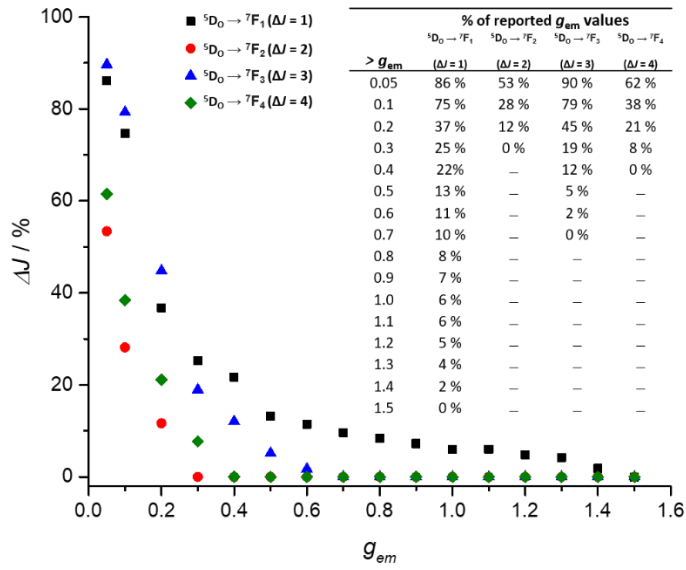


Figure 6 | **Relative proportion of Eu^{III} g_{em} values reported in the literature for each emission band.** Each emission band shows a distinct a negative exponential trend as g_{em} increases.